

This discussion paper is/has been under review for the journal Geoscientific Model Development (GMD). Please refer to the corresponding final paper in GMD if available.

# Characterising Brazilian biomass burning emissions using WRF-Chem with MOSAIC sectional aerosol

S. Archer-Nicholls<sup>1</sup>, D. Lowe<sup>1</sup>, E. Darbyshire<sup>1</sup>, W. T. Morgan<sup>1</sup>, M. M. Bela<sup>2</sup>,  
G. Pereira<sup>3</sup>, J. Trembath<sup>4,1</sup>, J. W. Kaiser<sup>5,6,7</sup>, K. M. Longo<sup>8</sup>, S. R. Freitas<sup>8,9</sup>,  
H. Coe<sup>1</sup>, and G. McFiggans<sup>1</sup>

<sup>1</sup>Centre for Atmospheric Sciences, School of Earth, Atmospheric and Environmental Sciences, University of Manchester, Manchester, UK

<sup>2</sup>Laboratory for Atmospheric and Space Physics, University of Colorado, Boulder, USA

<sup>3</sup>Department of Geoscience (DEGEO), Federal University of São João del Rei (UFSJ), São João del Rei, Brazil

<sup>4</sup>Facility for Airborne Atmospheric Measurements (FAAM), Cranfield University, Bedfordshire, UK

<sup>5</sup>King's College London (KCL), London, UK

<sup>6</sup>European Centre for Medium-range Weather Forecasts, Reading, UK

<sup>7</sup>Max Planck Institute for Chemistry, Mainz, Germany

<sup>8</sup>Centre for Earth System Science (CCST), National Institute for Space Research (INPE), São José dos Campos, Brazil

GMDD

7, 6061–6131, 2014

## SAMBBA WRF-Chem setup

S. Archer-Nicholls et al.

[Title Page](#)

[Abstract](#)

[Introduction](#)

[Conclusions](#)

[References](#)

[Tables](#)

[Figures](#)

◀

▶

◀

▶

[Back](#)

[Close](#)

[Full Screen / Esc](#)

[Printer-friendly Version](#)

[Interactive Discussion](#)



Received: 4 September 2014 – Accepted: 8 September 2014 – Published: 17 September 2014

Correspondence to: G. McFiggans (g.mcfiggans@manchester.ac.uk)

Published by Copernicus Publications on behalf of the European Geosciences Union.

---

**SAMBBA WRF-Chem setup**

---

S. Archer-Nicholls et al.

---

[Title Page](#)

[Abstract](#)

[Introduction](#)

[Conclusions](#)

[References](#)

[Tables](#)

[Figures](#)

◀

▶

◀

▶

[Back](#)

[Close](#)

[Full Screen / Esc](#)

[Printer-friendly Version](#)

[Interactive Discussion](#)



## Abstract

The South American Biomass Burning Analysis (SAMBBA) field campaign took detailed in-situ flight measurements of aerosol during the 2012 dry season to characterise biomass burning aerosol and improve understanding of its impacts on weather and climate. Developments have been made to the Weather research and Forecast model with chemistry (WRF-Chem) model to improve the representation of biomass burning aerosol in the region by coupling a sectional aerosol scheme to the plume rise parameterisation. Brazilian Biomass Burning Emissions Model (3BEM) fire emissions are used, prepared using PREP-CHEM-SRC, and mapped to CBM-Z and MO-SAIC species. Model results have been evaluated against remote sensing products, AERONET sites, and four case studies of flight measurements from the SAMBBA campaign.

WRF-Chem predicted layers of elevated aerosol loadings ( $5\text{--}20\text{ }\mu\text{g sm}^{-3}$ ) of particulate organic matter at high altitude (6–8 km) over tropical forest regions, while flight measurements showed a sharp decrease above 2–4 km altitude. This difference was attributed to the plume-rise parameterisation overestimating injection height. The 3BEM emissions product was modified using estimates of active fire size and burned area for the 2012 fire season, which reduced the fire size. The enhancement factor for fire emissions was increased from 1.3 to 5 to retain reasonable aerosol optical depths (AOD). The smaller fire size lowered the injection height of the emissions, but WRF-Chem still showed elevated aerosol loadings between 4–5 km altitude. Over eastern Cerrado (savannah-like) regions, both modelled and measured aerosol loadings decreased above approximately 4 km altitude.

Compared with MODIS satellite data and AERONET sites, WRF-Chem represented AOD magnitude well (between 0.3–1.5) over western tropical forest fire regions in the first half of the campaign, but tended to over-predict them in the second half, when precipitation was more significant. Over eastern Cerrado regions, WRF-Chem tended to under-predict AOD. Modeled aerosol loadings in the east were higher in the modified

## SAMBBA WRF-Chem setup

S. Archer-Nicholls et al.

[Title Page](#)

[Abstract](#)

[Introduction](#)

[Conclusions](#)

[References](#)

[Tables](#)

[Figures](#)

◀

▶

◀

▶

[Back](#)

[Close](#)

[Full Screen / Esc](#)

[Printer-friendly Version](#)

[Interactive Discussion](#)



emission scenario. The primary organic matter to black carbon ratio was typically between 8–10 in WRF-Chem. This was lower than western flights measurements (interquartile range of 11.6–15.7 in B734, 14.7–24.0 in B739), but similar to the eastern flight B742 (8.1–10.4). However, single scattering albedo was close to measured over the western flights (0.87–0.89 in model; 0.88–0.91 in flight B734, and 0.86–0.95 in flight B739 measurements) but too high over the eastern flight B742 (0.86–0.87 in model, 0.81–0.84 in measurements). This suggests that improvements are needed to both modeled aerosol composition and optical properties calculations in WRF-Chem.

5

## 1 Introduction

10 Biomass burning in South America is a globally significant source of carbonaceous aerosol (black carbon (BC) and organic carbon (OC)) (Streets et al., 2004). As well as seriously impacting on the health of the local population (Ignotti et al., 2010; de Andrade Filho et al., 2013), this biomass burning aerosol (BBA) influences the climate on a regional and global scale (Andreae et al., 2004; Zhang et al., 2009; Boucher et al., 2013). BBA can impact weather and climate directly, through interaction with radiation (Haywood and Boucher, 2000), and indirectly, by acting as cloud condensation nuclei (CCN), changing cloud optical properties, lifetime and capacity to initiate precipitation (McFiggans et al., 2006). Aerosol optical properties and suitability as CCN are both highly sensitive to the size distribution and composition of the aerosol population

15 (Bond and Bergstrom, 2006; Abdul-Razzak and Ghan, 2002; McFiggans et al., 2006). Modelling the impacts of BBA on a regional scale requires a fully coupled “online” approach, with detailed descriptions of the aerosol properties and two-way interactions between the aerosol, radiation and cloud processes (Grell and Baklanov, 2011).

20

High-quality emissions are essential for running chemical transport or coupled models. PREP-CHEM-SRC is a pre-processor, designed to combine data from multiple global emission databases to produce anthropogenic, biogenic and biomass burning gridded emission maps (Freitas et al., 2011). Originally developed for the

[Title Page](#)  
[Abstract](#) [Introduction](#)  
[Conclusions](#) [References](#)  
[Tables](#) [Figures](#)  
[◀](#) [▶](#)  
[◀](#) [▶](#)  
[Back](#) [Close](#)  
[Full Screen / Esc](#)  
[Printer-friendly Version](#)  
[Interactive Discussion](#)



CCATT-BRAMS model (Freitas et al., 2009; Longo et al., 2010), it has been extended for use with the Weather Research and Forecast model with Chemistry (WRF-Chem, Grell et al., 2011). PREP-CHEM-SRC can generate fire emissions using either the GFEDv2 inventory to produce 8 day averages (Van der Werf et al., 2006), or daily maps using the Brazilian Biomass Burning Emission Model (3BEM) (Longo et al., 2010). 3BEM has been shown to improve modelled predictions of CO compared to the lower-resolution GFEDv2 dataset (Longo et al., 2010).

Both of these inventories use a traditional “bottom-up” approach, whereby emissions for each species ( $[i]$ ) are estimated by multiplying emission factors ( $EF^{[i]}$ ) with an estimate of the burned biomass. Satellite data is used to quantify global fire activity in terms of fire count, observed burnt area or fire radiative power (FRP), and subsequently apply properties such as fuel load and combustion completeness from model calculations or limited field and laboratory measurements. The fire properties can be very difficult to measure, resulting in large uncertainties in the emissions (Van der Werf et al., 2010; Ichoku et al., 2012; Kaiser et al., 2012). Newer, “top-down” approaches to producing fire emissions systematically include information from large-scale smoke plume observations, e.g. in flux inversion from satellite observations (Huneeus et al., 2012; Ichoku and Ellison, 2013), or enhanced aerosols in Kaiser et al. (2012). These methods show a lot of promise for being able to produce near real-time fire emissions for air quality forecasting, although there are difficulties related to the retrieval algorithms and consistency between different data sources (Pereira et al., 2009). Measurements of FRP are also generally limited to cloud-free regions, and affected by the time of satellite passover and obstructions of line of sight to the fire, for example by tall trees (Kaiser et al., 2012). This can lead to biases in fire emissions in some regions of the globe (Andela et al., 2013).

The high temperatures of open vegetation fires produce flaming emissions with a lot of associated buoyancy. In large fires, the emitted air-mass may rise far above the planetary boundary layer, in some cases inducing convection forming so-called pyrocumulus clouds (Andreae et al., 2001). The height of the plume can vary hugely,

---

**SAMBBA WRF-Chem setup**

S. Archer-Nicholls et al.

[Title Page](#)[Abstract](#)[Introduction](#)[Conclusions](#)[References](#)[Tables](#)[Figures](#)[◀](#)[▶](#)[◀](#)[▶](#)[Back](#)[Close](#)[Full Screen / Esc](#)[Printer-friendly Version](#)[Interactive Discussion](#)

depending on season, the biome being burned, atmospheric stability conditions and size of fire (Val Martin et al., 2010b). Many global models mix emissions within the boundary layer. For example, Dentener et al. (2006) provides recommended mixing heights for different biomass burning regions for global models: agricultural waste only in the lowest model levels, tropical fires in the lower 1 km, temperate fires in the lower 2 km and boreal up to 6 km. However, larger fires may penetrate above the boundary layer. Failing to account for these may result in the underestimation of emissions in the free troposphere (Ichoku et al., 2012).

A plume-rise parameterisation that can be embedded into regional transport models was developed by Freitas et al. (2007). The 1-D plume-rise parameterisation was initially implemented in the CCATT-BRAMS model (Freitas et al., 2009; Longo et al., 2010). Freitas et al. (2007) have shown improved representation of the vertical profile of carbon monoxide (CO) compared to measurements from the 2002 SMOCC campaign when using the plume-rise parameterisation. This parameterisation has been successfully ported into WRF-Chem (Grell et al., 2005), to be used with the RADM (Stockwell et al., 1990) or RACM (Stockwell et al., 1997) chemical mechanisms, and GOCART (Chin et al., 2000) or MADE/SORGAM (Ackermann et al., 1998) aerosol. It has been used in many studies, for example to investigate the impact of Alaskan wild-fires on weather forecasts (Grell et al., 2011); to study the effects of BBA on clouds, deep convection and precipitation in the Amazon (Wu et al., 2011a, b); and evaluating the impact of fire emissions on ozone ( $O_3$ ) formation (Bela et al., 2014).

While improvements have been observed when using the plume-rise parameterisation in some studies, care should be taken. There are difficulties in using a parameterisation to represent such a complex non-linear process, as the properties needed (such as fire size, buoyancy and entrainment rate) are difficult to quantify, potentially leading to large errors (Ichoku et al., 2012). Indications of the plume-rise over-predicting injection height have been observed. For example, Wu et al. (2011a) found clear-sky aerosol extinction levels between 800 and 100 hPa to be higher in WRF-Chem when comparing against CALIPSO satellite observations, although they were unsure how

## SAMBBA WRF-Chem setup

S. Archer-Nicholls et al.

[Title Page](#)

[Abstract](#)

[Introduction](#)

[Conclusions](#)

[References](#)

[Tables](#)

[Figures](#)

◀

▶

◀

▶

[Back](#)

[Close](#)

[Full Screen / Esc](#)

[Printer-friendly Version](#)

[Interactive Discussion](#)



much of this discrepancy was due to the plume-rise parameterisation and how much from convective transport. Val Martin et al. (2010b) found over 95 % of North American tropical forest fires plume injection heights measured using the MISR satellite to be less than 1.5 km, while Fig. 3 in Freitas et al. (2011) shows modelled mid-afternoon

5 South-America tropical forest emissions to have injection heights between 4 and 9 km.

Having aerosol injected into the wrong portion of the vertical column can have many implications. The main loss-processes for BBA are wash-out and wet-deposition (Taylor et al., 2014), therefore aerosol above cloud will likely remain in the atmosphere for longer and be transported further from source. In addition, the effect of BC on atmospheric heating rates is different at different altitudes, becoming more important aloft (Samset and Myhre, 2011; Ban-Weiss et al., 2011; Samset et al., 2013).

10 This study aims to critically evaluate the plume-rise parameterisation in WRF-Chem against in-situ flight measurements over Brazil. The work has been carried out as part of the South American Biomass Burning Analysis (SAMBBA) project, an international collaboration set up to better understand and reduce the uncertainties associated with the impacts of biomass burning in South America on regional and global climate, air quality, and ecosystems. The observational phase of SAMBBA consisted of an air-borne measurement campaign using the UK Facility for Airborne Atmospheric Measurement (FAAM) BAe-146 research aircraft (Morgan et al., 2013), alongside a longer

15 term ground based deployment (Brito et al., 2014).

20 The SAMBBA modelling campaign consists of a hierarchy of models across a range of scales, from the cloud-resolving to the global. WRF-Chem is being applied to better understand the properties and impacts of BBA at a regional scale. This study describes developments being made to the WRF-Chem model to improve the applicability of the model for this task. The MOdel for Simulating Aerosol Interactions with Chemistry (MOSAIC) (Zaveri et al., 2008) aerosol mechanism has been used with the plume-rise parameterisation in order to improve the physical description and size distribution of modelled BBA. Work has also been conducted to modify the input parameters used by

**SAMBBA WRF-Chem setup**

S. Archer-Nicholls et al.

[Title Page](#)

[Abstract](#)

[Introduction](#)

[Conclusions](#)

[References](#)

[Tables](#)

[Figures](#)

◀

▶

◀

▶

[Back](#)

[Close](#)

[Full Screen / Esc](#)

[Printer-friendly Version](#)

[Interactive Discussion](#)



the 3BEM emissions and the plume-rise parameterisation in order to better control the injection height of BB emissions.

Model runs in this study have been carried out using a modified version of WRF-Chem v3.4.1. Model results are critically assessed against remote measurements of aerosol optical depth (AOD), from satellites and ground based AERONET stations (Holben et al., 2001), and in-situ measurements from the BAe-146 aircraft campaign. This is aimed at characterising the horizontal and vertical distribution of the regional haze, evaluating the behaviour of the plume-rise parameterisation, and comparing the composition, size distribution and optical properties of the aerosol population with a high-resolution data source. With the aerosol distribution and properties characterised, the model setup can be justifiably used to investigate the impacts of the aerosol on regional weather and climate in future studies.

## 2 Model, emissions and the plume-rise parameterisation description

### 2.1 WRF-Chem and the sectional MOSAIC aerosol mechanism.

WRF-Chem is a regional, fully-coupled “online” model (Grell et al., 2005), where all prognostic meteorological, chemical and aerosol variables are integrated on the same timestep and are transported using the same advection and physical parameterisations. This makes it ideal for investigating the impacts of atmospheric composition on weather at a regional scale (Grell and Baklanov, 2011; Baklanov et al., 2014). There are several aerosol mechanisms available in WRF-chem. Of these, only MOSAIC (Zaveri et al., 2008) uses the more rigorous sectional representation of aerosol size distribution, enabling detailed aerosol interactions with radiation and clouds (Chapman et al., 2009). MOSAIC is only compatible with a subset of chemical mechanisms in WRF-Chem. For this study, the gas-phase mechanism used is CBM-Z (Zaveri and Peters, 1999).

[Title Page](#)

[Abstract](#)

[Introduction](#)

[Conclusions](#)

[References](#)

[Tables](#)

[Figures](#)

[◀](#)

[▶](#)

[◀](#)

[▶](#)

[Back](#)

[Close](#)

[Full Screen / Esc](#)

[Printer-friendly Version](#)

[Interactive Discussion](#)



The aerosol size distribution in MOSAIC is described by size bins spanning a dry particle diameter ( $D_p$ ) range of 39 nm to 10  $\mu\text{m}$ . In 8-bin mode the bin bounds increase geometrically by a factor of two for each bin, as shown in Table 2. The chemical constituents of the aerosol are assumed to be internally mixed within bins, and externally mixed between bins. MOSAIC carries five inorganic ions, plus three other aerosol species: black carbon (BC); particulate organic mass (POM); and other inorganics (OIN), which includes crustal and dust particles (Zaveri et al., 2008). Secondary organic aerosol (SOA) has been incorporated into MOSAIC using the volatility basis set (VBS) (Shrivastava et al., 2011, 2013). However, this is still under development and aerosol-radiative interactions have not yet been included. It is currently unclear how much of an impact including SOA formation has on aerosol composition in regions heavily effected by biomass burning emissions. Some recent evidence suggests that, after the first few minutes of ageing, there is little SOA formation. For example, Jolleys et al. (2012) show the POM : CO ratio is conserved downwind of fires and likely determined at source, depending on the fuel type and burning conditions. However, Vakkari et al. (2014), found SOA formation in the first 2–4 h of plume ageing to be a significant contributor to BBA composition and properties.

The optical properties of an aerosol population depend on the chemical composition and size distribution (Barnard et al., 2010). Interactions with radiation are most efficiently when the diameter is of the same order as the wavelength ( $\lambda$ ) of the incident light, typically a few hundred nm for visible light (Bond and Bergstrom, 2006). The most important chemical component in determining optical properties is BC, due to the high imaginary component of its complex refractive index ( $1.95 - 0.79i$  at 550 nm, as recommended by Bond and Bergstrom, 2006). The absorbing properties of BC can be enhanced by the non-absorbing aerosol components with which it is mixed (Bond et al., 2006, 2013). To simulate this, a “mixing-rule” is employed to calculate the bulk complex refractive index of each bin (Ackermann and Toon, 1982; Bond et al., 2006). Three mixing-rules are available in WRF-Chem: volume averaging, where the BC is evenly mixed with the other components; Maxwell–Garnet, where the BC is seen as small,

## SAMBBA WRF-Chem setup

S. Archer-Nicholls et al.

[Title Page](#)

[Abstract](#)

[Introduction](#)

[Conclusions](#)

[References](#)

[Tables](#)

[Figures](#)

◀

▶

◀

▶

[Back](#)

[Close](#)

[Full Screen / Esc](#)

[Printer-friendly Version](#)

[Interactive Discussion](#)



randomly distributed particles; and Shell–Core, where the BC forms the core of each particle, surrounded by a “shell” of everything else. Bond et al. (2006) strongly recommend not using a volume-averaging mixing rule, as it tends to artificially overestimate the absorption enhancement of BC.

5 Mie calculations are used to first find the optical properties of each bin (Toon and Ackerman, 1981), then summed over all bins to give the bulk optical properties of the aerosol population: the extinction, ( $b_{\text{ext}}$ ), scattering coefficient ( $b_{\text{scat}}$ ), absorption coefficient ( $b_{\text{abs}}$ ), single scattering albedo ( $\omega_0$ ) and asymmetry factor for scattering ( $g$ ). Each of these is defined as a function of  $\lambda$ , with  $\omega_0$  being the ratio of scattering to extinction:

$$\omega_0 = \frac{b_{\text{scat}}}{b_{\text{scat}} + b_{\text{abs}}} = \frac{b_{\text{scat}}}{b_{\text{ext}}}. \quad (1)$$

Full descriptions of the aerosol optical calculations in WRF-Chem are described by Fast et al. (2006) and Barnard et al. (2010).

15 Recent WRF-Chem developments have enabled explicit modelling of the mixing state of BC with other components (Matsui et al., 2013). These have shown internal mixing-rule approximations to overestimate the radiative absorption of aerosol by 30–40 % in the boundary layer. This treatment is, however, extremely computationally expensive to run.

20 Within WRF-Chem it is assumed that the organic fraction of the aerosol is non-absorbing in the short-wave. However, there is some evidence of POM, particularly in BBA, weakly absorbing radiation at some wavelengths (known as brown carbon, BrC; Lack et al., 2012, 2013; Saleh et al., 2014). Saleh et al. (2014) suggest BrC absorption can be parameterised using a relation between the POM:BC ratio. Weak short-wave absorption by POM may need to be added in future versions of WRF-Chem to model BBA optical properties accurately.

[Title Page](#)[Abstract](#)[Introduction](#)[Conclusions](#)[References](#)[Tables](#)[Figures](#)[◀](#)[▶](#)[◀](#)[▶](#)[Back](#)[Close](#)[Full Screen / Esc](#)[Printer-friendly Version](#)[Interactive Discussion](#)

## 2.2 Brazilian biomass burning emissions model

The 3BEM fire emissions product uses daily data of detected fires from several satellite products: the Moderate Resolution Imaging Spectroradiometer (MODIS) (Giglio et al., 2003), the Geostationary Operational Environmental Satellite-Wildfire Automated Biomass Burning Algorithm (GOES WFABBA, [cimss.ssec.wisc.edu/goes/burn/wfabba.html](http://cimss.ssec.wisc.edu/goes/burn/wfabba.html); Prins et al., 1998) and the Brazilian National Institute for Space Research (INPE) fire product, which uses the Advanced Very High Resolution Radiometer (AVHRR) on-board the NOAA polar orbiting satellite series ([www.cptec.inpe.br/queimadas](http://www.cptec.inpe.br/queimadas); Setzer and Pereira, 1991). A filter algorithm that removes fires within 1 km of each other is used to prevent double counting between datasets (Longo et al., 2010).

Each fire pixel is cross-referenced against 1 km resolution maps of vegetation and land-use for the year 2000 (Olson et al., 2000; Sestini et al., 2003). The fire is assigned one of four different biomes: tropical forest, extra-tropical forest, savannah/cerrago, or grassland. Different carbon density ( $\alpha$ ) and combustion factors ( $\beta$ ) are used for each biome type, and are multiplied to find the total burned biomass. Each biome type also has associated emission factors ( $EF_{veg}^{[i]}$ ) of Andreae and Merlet (2001), to convert from mass of biomass burned to quantity of each emitted species ( $[i]$ ). These are further scaled by an estimated total burned area ( $A_{fire}$ ). The burned area cannot be directly measured from satellite products in real time, although it may be estimated from fire radiative product (FRP) using an algorithm, if suitable data is available. An average area burned is often used due to difficulties in quickly retrieving accurate readings from satellite products. Some fires detected by the WFABBA product have  $A_{fire}$  estimated using the Dozier method (Dozier, 1981, <http://wfabba.ssec.wisc.edu/ongoing.html>). If this data is not available (as is the case for fire detected with the MODIS and INPE products), an average fire size of 22.8 ha is used for all vegetation types (Longo et al., 2010). Finally, the fire emissions may need to be scaled up by an enhancement factor ( $f_x$ ) in order to account for uncertainties and produce physically realistic aerosol optical

## SAMBBA WRF-Chem setup

S. Archer-Nicholls et al.

[Title Page](#)

[Abstract](#)

[Introduction](#)

[Conclusions](#)

[References](#)

[Tables](#)

[Figures](#)

◀

▶

◀

▶

[Back](#)

[Close](#)

[Full Screen / Esc](#)

[Printer-friendly Version](#)

[Interactive Discussion](#)



depths (AODs). These factors are combined to give the emitted mass of each species:

$$M^{[i]} = \alpha_{\text{veg}} \cdot \beta_{\text{veg}} \cdot \text{EF}_{\text{veg}}^{[i]} \cdot A_{\text{fire}} \cdot f_x. \quad (2)$$

By default,  $f_x$  is set to 1.3 for South American fires in PREP-CHEM-SRC v1.4. Enhancement factors such as this have been applied to many emission products and models, in order to bring bottom-up inventories in line with top-down constraints (Kaiser et al., 2012; Tosca et al., 2013) fire emission inventories. Values in the literature typically range from 2 to 5. For example, Wu et al. (2011a) multiplied 3BEM OC and BC surface aerosol emissions by a factor of 5 when simulating the 2006 fire season. Tosca et al. (2013) used an enhancement factor of 2.4 for South American fires using the GFEDv3 inventory with the CAM-5 model, and Kaiser et al. (2012) recommend scaling GFASv1.0 particulate emissions by a factor of 3.4. The need for this factor highlights the difficulties and uncertainties in estimating fire emissions using the currently available observations and understanding of the processes involved. Petrenko et al. (2012) demonstrate that the required factor depends strongly on the underlying emission inventory and the geographical location.

### 2.3 Plume rise parameterisation

The Freitas et al. (2007) plume-rise parameterisation applies a 1-D cloud-resolving model to each grid-column within the WRF-Chem model domain that contains a fire. It calculates the initial plume buoyancy by estimating the energy and moisture released from the fire, based on fire size and carbon density, and using ambient environmental conditions along the column retrieved from the parent model. The plume rises until it becomes dynamically stable, and the height at this point is passed to the parent model. The microphysical parameterisation of Kessler (1969), with accretion and ice formation of Ogura and Takahashi (1971), is used to compute whether convection occurs, the latent energy released and the effect on the height of the plume, using an initial cloud condensation nuclei (CCN) concentration of  $10^5 \text{ cm}^{-3}$  taken from Andreae et al. (2004).

[Title Page](#)[Abstract](#)[Introduction](#)[Conclusions](#)[References](#)[Tables](#)[Figures](#)[|◀](#)[▶|](#)[◀](#)[▶](#)[Back](#)[Close](#)[Full Screen / Esc](#)[Printer-friendly Version](#)[Interactive Discussion](#)

The total fire emissions are split between smouldering and flaming phases, with the fraction apportioned depending on the vegetation being burned. A lower and upper estimate of heat flux is used to give lower and upper limits of the injection height. The flaming fraction is emitted between these elevated injection heights, while smouldering emissions are emitted into the lowest mode level (Freitas et al., 2007).

The behaviour of the plume-rise parameterisation is dependent on the location and size of each fire. The heat flux and flaming fractions of the fires differ for each of the four biomes, with forest fires burning more energetically than savannah or grassland fires due to higher carbon density (Freitas et al., 2007). The main loss of buoyancy results from entrainment of colder air from the surrounding environment into the plume:

$$\frac{\partial w}{\partial t} + w \frac{\partial w}{\partial z} = -(\lambda_{\text{entr}} + \delta_{\text{entr}})w, \quad (3)$$

where  $w$  is the vertical speed of the plume, and  $\lambda_{\text{entr}}$  and  $\delta_{\text{entr}}$  are the lateral and shear entrainment terms respectively.  $\lambda_{\text{entr}}$  is given by:

$$\lambda_{\text{entr}} = \frac{2\alpha}{R}|w|, \quad (4)$$

where  $R$  is the radius of the plume,  $w$  the vertical velocity of the plume and  $\alpha$  the dynamic entrainment constant (Freitas et al., 2007), taken to be 0.05 for good agreement with the Active Tracer High resolution Atmospheric Model (ATHAM) model simulations

(Freitas et al., 2010). Freitas et al. (2010) have expanded the parameterisation to include entrainment of shear wind as well as vertical:

$$\delta_{\text{entr}} = \frac{2}{\pi R}(u_e - u), \quad (5)$$

where  $u$  and  $u_e$  are the horizontal wind speeds of the plume and environmental respectively. Note that  $(u_e - u)$  in Eq. (5) is formulated as a scalar difference. This implicitly assumes the environmental and plume winds are in the same direction. A vector difference would account for changes in wind direction in the vertical column. The current

<a href="#">Title Page</a>	
<a href="#">Abstract</a>	<a href="#">Introduction</a>
<a href="#">Conclusions</a>	<a href="#">References</a>
<a href="#">Tables</a>	<a href="#">Figures</a>
<a href="#">◀</a>	<a href="#">▶</a>
<a href="#">◀</a>	<a href="#">▶</a>
<a href="#">Back</a>	<a href="#">Close</a>
<a href="#">Full Screen / Esc</a>	
<a href="#">Printer-friendly Version</a>	
<a href="#">Interactive Discussion</a>	



formulation therefore systematically underestimates the horizontal entrainment effect, although the difference is likely to be small in most cases.

The plume radius  $R$  is derived from the active size of the fire ( $S_{\text{fire}}$ ), assuming the cross-section of the plume to be circular (i.e.  $R \propto \sqrt{S_{\text{fire}}}$ ). As both  $\lambda_{\text{entr}}$  and  $\delta_{\text{entr}}$  are inversely proportional to  $R$ , larger fires undergo less entrainment and have higher injection heights (Freitas et al., 2010). The full set of equations for plume dynamics, microphysics and entrainment are described in detail by Freitas et al. (2007, 2010).

### 3 Model and emission product developments

This section of the paper presents development work carried out to improve BBA representation within WRF-Chem with sectional aerosol. The developments can be summarised as:

1. PREP-CHEM-SRC was modified to use updated fire size data for the 2012 fire season when generating 3BEM emissions. This information was fed to the plume-rise parameterisation to achieve more realistic injection heights.
2. Gas-phase emissions from PREP-CHEM-SRC were mapped to CBM-Z species, and aerosol emissions to MOSAIC sectional aerosol with appropriate size distributions.
3. Boundary conditions derived from the MACC-II product were added to capture long-range transport of BBA into the regional model domain.

#### 20 3.1 Updating fire size estimates for the 2012 biomass burning season

The plume-rise parameterisation in WRF-Chem shows a tendency towards overestimating the injection height of flaming emissions, as will be shown in the results section in this paper. Ichoku et al. (2012) suggest restraining the plume height using remote measurements of plume height, such as the MISR satellite. For this work, the inputs of

[Title Page](#)

[Abstract](#)

[Introduction](#)

[Conclusions](#)

[References](#)

[Tables](#)

[Figures](#)

◀

▶

◀

▶

[Back](#)

[Close](#)

[Full Screen / Esc](#)

[Printer-friendly Version](#)

[Interactive Discussion](#)



the parameterisation have been refined in the aim of improving the predictive capacity of the injection height calculation.

There are several assumptions built into the 3BEM emissions and plume-rise setup which may make it prone to having a positive bias. Firstly, there has been a downward trend in fire emissions since the late 1990s and early 2000s (Artaxo et al., 2013). Much of the evaluation of the plume-rise parameterisation and 3BEM emissions product has used data from 2002 (Freitas et al., 2007, 2009; Longo et al., 2010). In using the relatively large estimate of the average burned area for all fires of 22.8 ha, we may be simulating overly large fires more representative of the previous decade than the modern day. Secondly, the active fire size ( $S_{\text{fire}}$ ) used by the plume-rise parameterisation is the same as the total burned area ( $A_{\text{fire}}$ ) used to calculate the emitted mass (i.e.  $A_{\text{fire}} = S_{\text{fire}}$ ). Logically, it is not reasonable to assume that the actively burning portion of a fire is the same as the total burned area. It is known that fires spread along a front (Viegas, 1998), and this behaviour should be approximated in the equations used to calculate the plume-rise.

A number of methods for deriving fire size from satellite products have been developed. Dozier (1981) proposed a bi-spectral approach that utilises the estimated radiance at 4 and 11  $\mu\text{m}$ . However, inaccuracies in data acquisition and the digital processing required (for example, co-registration between bands with distinct spatial resolutions and point spread functions, sensor noise and spectral atmospheric interference) could generate large errors in fire size estimation (Giglio and Kendall, 2001; Giglio and Justice, 2003). As a consequence a number of modifications to the Dozier method have been proposed (Peterson and Wang, 2013; Peterson et al., 2013; Shimabukuro et al., 2013; Giglio and Schroeder, 2014). However, fires which occur within the biomes specific to the Amazon and Cerrado regions present distinct behaviours (Arai et al., 2011) for which the majority of these schemes have not been calibrated and validated.

For this study, updated estimates of burned area for the 2012 season have been used, acquired from a pre-operational product of CPTEC/INPE (Shimabukuro et al., 2013). In this product, burned area and active fire size are estimated through FRP

[Title Page](#)[Abstract](#)[Introduction](#)[Conclusions](#)[References](#)[Tables](#)[Figures](#)[◀](#)[▶](#)[◀](#)[▶](#)[Back](#)[Close](#)[Full Screen / Esc](#)[Printer-friendly Version](#)[Interactive Discussion](#)

and Fire Radiative Energy (FRE) based coefficients to different types of vegetation in South America (grassland, herbaceous, scrublands, forest, and agriculture), derived from simultaneous observations of Thematic Mapper (TM) and Enhanced Thematic Mapper Plus (ETM+) images of Landsat 5 and Landsat 7, respectively. MODIS FRP values were used to estimate the fire size using:

$$\text{GRID}_{(\text{lon}, \text{lat}, \text{FRP}, \text{LULC})} = \sum_{x=-\alpha}^{\alpha} \sum_{y=-\beta}^{\beta} (\vartheta(x, y) \text{FRP}(\text{lon} + x, \text{lat} + y) \cap \vartheta(x, y) \text{LULC}(\text{lon} + x, \text{lat} + y)) A_c, \quad (6)$$

where  $\vartheta(x, y)$  represents the convolution mask of  $M \times N$  size (rows  $\times$  columns), FRP is the estimated MODIS FRP derived from MOD14 and MYD14 products, LULC is the land cover type derived from MCD12Q1 product, and  $A_c$  is the fire size coefficient (0.00021–0.00029  $\text{km}^2 \text{MW}^{-1}$ ). GRID is the fire size ( $S_{\text{fire}}$ ) defined for all points which the mask of  $M \times N$  size completely overlaps the grid ( $\text{lon} \in [\alpha, M - \alpha]$ ,  $\text{lat} \in [\beta, N - \beta]$ ). The same approach is applied to derive  $A_{\text{fire}}$  by replacing FRP with FRE, as described in Shimabukuro et al. (2013).

Table 1 shows estimates of mean  $A_{\text{fire}}$  and  $S_{\text{fire}}$  for the 2012 Brazilian fire season, made using the above method. The estimates are dependent on biome (in a similar fashion to  $\text{EF}_{\text{veg}}^{[i]}$ ,  $\alpha_{\text{veg}}$  and  $\beta_{\text{veg}}$  in Eq. 2). As the data was collated for South America over 2012, it should provide more representative estimates of burned area and fire size for the SAMBBA study, given the downward trend in fires over the past decade.  $S_{\text{fire}}$  is some 10 to 20 times smaller than 22.8 ha, depending on the biome, meaning the entrainment rate is increased by a factor between 3 and 5. The modified 3bem\_emissions.f90 code for PREP-CHEM-SRC v1.4 is included in the Supplement, with instructions on how to modify for another campaign.

Reducing the estimated  $A_{\text{fire}}$  to a more reasonable size also reduces the total emitted mass. It was found that this resulted in unrealistically low aerosol optical depths (AODs). Previous models have used higher factors to get reasonable AODs

[Title Page](#)[Abstract](#)[Introduction](#)[Conclusions](#)[References](#)[Tables](#)[Figures](#)[◀](#)[▶](#)[◀](#)[▶](#)[Back](#)[Close](#)[Full Screen / Esc](#)[Printer-friendly Version](#)[Interactive Discussion](#)

as discussed above. For this study  $f_x$  has been increased from 1.3 to 5. This has been estimated based on the reduction of tropical forest  $A_{\text{fire}}$  by approximately a factor of 5 from the original default area of 22.8 ha, while the other biomes are between a third and half the size. As forest fires are the dominant source of emissions in the region, this maintains similar magnitudes of particulate emissions so the study can focus on the implications of the injection height changes.

### 3.2 Coupling PREP-CHEM-SRC emissions with CBM-Z MOSAIC

The emissions generated by PREP-CHEM-SRC are made with the RADM2 and GO-CART speciation. For the gas-phase emissions we have ported the mappings used for anthropogenic RADM2 speciations to CBM-Z within WRF-Chem. The excess carbon from longer chained hydrocarbons are added to the CBM-Z species PAR, OLET and OLEI, as described in Zaveri and Peters (1999). BBA emissions for MOSAIC have been treated differently from anthropogenic emissions within the emission subroutine. While anthropogenic emissions are only injected into the lower most levels, BB emissions loop through the entire vertical column in order to distribute flaming emissions using the injection heights calculated by the plume-rise parameterisation.

Emissions of BBA are usually observed in two size modes, a sub-micron accumulation mode which makes up the majority of the particulate number and mass, plus a coarse mode made up of a lower number of larger particles (Reid and Hobbs, 1998).

The fine mode is mostly organic compounds, with around 10 % BC and inorganic species respectively. The coarse mode is made up of dust, ash, carbon aggregates and unburned fuel (Reid et al., 2005; Janhäll et al., 2010). PREP-CHEM-SRC produces emission values for BC, OC,  $\text{PM}_{2.5}$  and  $\text{PM}_{10}$ , based on the factors in Andreae and Merlet (2001). For this study all BC and OC are assumed to be included in the  $\text{PM}_{2.5}$  fraction of emissions. The emissions of Organic Carbon (OC) need to be converted to total particulate organic matter (POM), which includes the associated oxygen, hydrogen and other elements. Biomass burning OC emissions have been converted to POM, multiplying by a factor of 1.5, following Reid et al. (2005). Similarly anthropogenic

Title Page

Abstract

Introduction

Conclusions

References

Tables

Figures

◀

▶

◀

▶

Back

Close

Full Screen / Esc

Printer-friendly Version

Interactive Discussion



OC emissions have been multiplied by a factor of 1.6 (Turpin and Lim, 2001) to yield POM. All emitted particulate mass that is not BC or POM is assumed to be unreactive inorganic in composition, and mapped to other inorganics (OIN).

Evidence from measurements of very fresh plumes suggest that in the few seconds after burning, there are a large number of small particles which rapidly coagulate (Reid and Hobbs, 1998). After a few minutes, the distribution generally has a single large accumulation mode, sometimes with a smaller coarse mode (Janhäll et al., 2010). Recent measurements of Vakkari et al. (2014) suggest significant changes to CCN, size distribution and  $\omega_0$  over the first 2–4 h of ageing through SOA formation in South African biomass burning plumes. However, these processes cannot currently be parameterised within this version of the model. A geometric mean diameter ( $D_g$ ) of 117 nm, with a geometric standard deviation ( $\sigma_g$ ) of 1.7, has been used to create a log-normal size distribution based on the average of 20 data points of fresh (no more than a few minutes old) smoke samples taken across several studies, compiled by Janhäll et al. (2010). This number distribution was converted to a volume distribution, normalised and, assuming a constant particle density, mapped to the 8 MOSAIC size bins. The fraction of total aerosol emissions assigned to each bin is shown in Table 2.

Biomass burning events exhibit a strong diurnal cycle (Giglio, 2007). To approximate this diurnal variation in a model, a gaussian with peak at a local time of around 15:00 LT (approximately 18:00 UTC over Brazil) is often used (Kaiser et al., 2009; Freitas et al., 2011). As a large landmass such as South America spans several time zones, for this work a local time ( $t_l$ ) for each emission point is calculated:

$$t_l = t_{\text{UTC}} + \frac{\text{LON}}{15} \quad (7)$$

where LON is the local longitude, in degrees, varying between  $-180^\circ$  and  $+180^\circ$ . This is used to define a gaussian function,  $r(t_l)$ , based on that used by Freitas et al. (2011), with a peak at 15:00 LT, defined such that the integral of  $r(t_l)$  over 24 h is equal to 1. This function modulates the magnitude of the emissions online within WRF-Chem. While Giglio (2007) suggest different diurnal cycles in different regions of Brazil based

[Title Page](#)

[Abstract](#)

[Introduction](#)

[Conclusions](#)

[References](#)

[Tables](#)

[Figures](#)

◀

▶

◀

▶

[Back](#)

[Close](#)

[Full Screen / Esc](#)

[Printer-friendly Version](#)

[Interactive Discussion](#)



on different biomes, it was considered problematic to extrapolate from the regions used in the study to the biomes used in PREP-CHEM-SRC, and so the single diurnal cycle of Freitas et al. (2011) was retained.

### 3.3 MACC-II boundary conditions

5 Whilst regional models benefit from the increased resolution allowed by simulating a smaller area, they are dependent on boundary conditions from global model datasets for everything occurring outside the domain bounds. There is evidence for dust and BBA from Africa being transported across the Atlantic to Brazil (Rizzo et al., 2013; Brito et al., 2014). Amazonian fire plumes may also be transported out of and recirculated back into the domain. In order to avoid simulating the whole of the Atlantic and 10 Africa, as was done by Freitas et al. (2009), it is necessary to be confident that the emission and long-range transport of these events is well captured by our boundary conditions.

15 The series of GEMS, MACC and MACC-II (Monitoring Atmospheric Composition and Climate – Interim Implementation Hollingsworth et al., 2008; Flemming et al., 2013) projects have developed analysis, reanalysis and forecast products that use the MOZART-3 chemical transport model (Emmons et al., 2010) with the ECMWF Integrated Forecast System (IFS), which has been expanded to integrate measurements of reactive gases, greenhouse gases and aerosol in the ECMWF 4D-Var assimilation 20 system (see Stein et al., 2012; Inness et al., 2013, and references therein). MODIS retrievals of aerosol optical depth at 550 nm are used to constrain modelled aerosol, improving its spatial distribution (Benedetti et al., 2009). Satellite retrieval columns of reactive gases ( $O_3$ , CO,  $NO_x$ , HCHO and  $SO_2$ ) are also assimilated (Stein et al., 2012). Daily biomass burning emissions of the Global Fire Assimilation System (GFAS) 25 (Kaiser et al., 2009, 2012) are used. Using daily fire emissions and satellite assimilation gives better constraint on the chemical and aerosol loadings, providing more reliable boundary conditions.

[Title Page](#)

[Abstract](#)

[Introduction](#)

[Conclusions](#)

[References](#)

[Tables](#)

[Figures](#)

◀

▶

◀

▶

[Back](#)

[Close](#)

[Full Screen / Esc](#)

[Printer-friendly Version](#)

[Interactive Discussion](#)



## SAMBBA WRF-Chem setup

S. Archer-Nicholls et al.

Title Page

Abstract

Introduction

Conclusions

References

Tables

Figures

◀

▶

◀

▶

Back

Close

Full Screen / Esc

Printer-friendly Version

Interactive Discussion



Only a subset of chemical species thought to be significant in long-range transport and chemistry are included in the MACC-II product: CO, O<sub>3</sub>, OH, SO<sub>2</sub>, NO<sub>2</sub>, HNO<sub>3</sub>, CH<sub>4</sub>, C<sub>2</sub>H<sub>6</sub>, isoprene, peroxyacetyl nitrate (PAN) and formaldehyde (HCHO). The aerosol module used in MACC-II is described by Morcrette et al. (2009). Five species of aerosol are carried: natural sea salt (SU) and dust (DU), and three anthropogenic aerosol (POM, BC and SULF). SULF, POM and BC are each treated as bulk aerosol, with BC and POM treated as two components – hydrophobic and hygrophilic. SS and DU are each represented with by bins with boundaries at 0.03, 0.5, 5 and 20 µm diameter for SS and 0.03, 0.55, 0.9 and 20 µm for DU (Morcrette et al., 2009).

The model uses log-normal distributions with parameters of mean diameter ( $D_p$ ) and geometric standard deviation ( $\sigma$ ) as defined below (Jean-Jaques Morcrette, personal communication, 2013):

- SS: two log-normal distributions; the first with  $D_{p,1} = 0.389\text{ }\mu\text{m}$ ,  $\sigma_{p,1} = 1.9$ ,  $N_{\text{tot},1} = 70$ , the second with  $D_{p,2} = 3.984\text{ }\mu\text{m}$ ,  $\sigma_{p,2} = 2.0$ ,  $N_{\text{tot},2} = 3$ .
- DU: a single log-normal distribution,  $D_p = 0.58\text{ }\mu\text{m}$ ,  $\sigma_p = 2.0$ .
- The bulk aerosol BC, POM and SO<sub>4</sub><sup>2-</sup> is assumed to be in an accumulation mode with single log-normal distribution,  $D_p = 0.071\text{ }\mu\text{m}$ ,  $\sigma_p = 2.0$ .

The fraction of each MACC-II bin to be partitioned into each MOSAIC bin is given by the fraction of each distribution that falls between each MOSAIC bin boundary. As the upper limit of MOSAIC aerosol is 10 µm, all aerosol mass from the distributions above 10 µm is discarded. See Table 3 for full apportionment to each MOSAIC size bin.

The SULF carried in MACC-II is assumed to be ammonium sulphate ((NH<sub>4</sub>)<sub>2</sub>SO<sub>4</sub>) when mapped to the WRF-Chem MOSAIC species, in order for the aerosol to have neutral acidity. Likewise, SS is assumed to be NaCl and is split between the Na<sup>+</sup> and Cl<sup>-</sup> ions. The MACC-II boundary conditions were interpolated to the model grid using a modified version of the mozbc script ([www.acd.ucar.edu/wrf-chem](http://www.acd.ucar.edu/wrf-chem)).

## 4 Campaign description

The SAMBBA aircraft campaign was based in Porto Velho, northern Rondônia. This is a region with extensive biomass burning owing to forest clearance. The ground measurement site was also located in the city, upwind of urban emissions. Nineteen flights were conducted between the 14 September and 3 October 2012, encompassing not only an extensive geographic area, but also differing synoptic conditions (see Darbyshire et al., 2014, for further details). Flights over the western regions encompassed two meteorological regimes as discussed in Brito et al. (2014), with Phase I (6 to 22 September 2012) representative of dry season conditions and Phase II (after 22 September) of the transition to the wet season. Comparatively, conditions remained dry throughout in the eastern Cerrado region.

### 4.1 Observational datasets

In this study, WRF-Chem model results are compared against various remote sensing and ground based datasets. The Tropical Rainfall Measuring Missions (TRMM) is a NASA project aiming to provide satellite derived estimates of tropical precipitation across the globe. The 3B42 product produces 3 hourly merged high quality, infrared and microwave precipitation estimates at  $0.25^\circ \times 0.25^\circ$  resolution between  $50^\circ$  N and  $50^\circ$  S (Huffman et al., 2001, 2013).

The Moderate Resolution Imaging Spectrometer (MODIS) instrument, on board the two NASA satellites Aqua and Terra, provide measurements of Aerosol Optical Depth (AOD) across a wide spectral range at  $1.0^\circ \times 1.5^\circ$  (Remer et al., 2005). For this study, retrievals of AOD at 550 nm are used for verifying the model aerosol horizontal distribution. Overpasses over the study period and region of the globe were at approximately 03:00 and 15:00 UTC for the Terra satellite, and 06:00 and 18:00 UTC for the Aqua satellite. Model data was extracted at the these times when comparing against MODIS data. Over land, the MODIS AOD retrievals have an error of approximately 0.05 (Remer et al., 2005).

[Title Page](#)[Abstract](#)[Introduction](#)[Conclusions](#)[References](#)[Tables](#)[Figures](#)[◀](#)[▶](#)[◀](#)[▶](#)[Back](#)[Close](#)[Full Screen / Esc](#)[Printer-friendly Version](#)[Interactive Discussion](#)

The Aerosol RObotic NETwork (AERONET) program is a ground-based deployment of around 100 sites, providing continuous observations of AOD at various wavelengths using the Version 2 Direct Sun Algorithm (Holben et al., 1998, 2001). AOD at 550 nm is estimated using measurements of AOD at 675 and 440 nm and the Angström component.

5 The data has been screened for clouds; only level 2.0 quality assured data is used for this study. Under cloud free conditions, the error in measured AOD is approximately 0.01 (Holben et al., 2001). Data was retrieved for four sites over the central Brazilian region: Cuiabá (15° S, 56° W), Ji Paraná (10° S, 61° W), Porto Vehlo (8° S, 63° W) and Rio Branco (9° S, 67° W).

## 10 4.2 Instrument details

The suite of aerosol instrumentation used on the FAAM BAe-146 for this study is summarised in Table 5. The submicron nonrefractory aerosol composition was measured by an Aerodyne Research (Billerica, MA, USA) compact Time of Flight Aerosol Mass Spectrometer (cToF-AMS), as described by Drewnick et al. (2005); Canagaratna et al. (2007), and for FAAM operation by Morgan et al. (2009). For speciated mass loadings, 15 detection limits are approximately  $40 \text{ ng m}^{-3}$  for organics (Drewnick et al., 2009), whilst combined measurement uncertainties are approximately 30 % (Bahreini et al., 2009; Middlebrook et al., 2012).

The Single Particle Soot Photometer (SP2), developed by Droplet Measurement 20 Technologies (Boulder, CO, USA), was used to measure number and mass concentrations of refractory Black Carbon (rBC). Its operating principles are described in Stephens et al. (2003) and Baumgardner et al. (2004), with its utilisation onboard FAAM summarised by McMeeking et al. (2010). For reported mass loadings the measurement uncertainty is approximately 30 % (Schwarz et al., 2008; Shiraiwa et al., 2008).

25 Aerosol total scattering coefficients were measured by a TSI Inc (St. Paul, MN, USA) 3-wavelength integrating nephelometer (Anderson et al., 1996), with standard corrections applied for angular truncation and non-lambertian light source errors (Anderson and Ogren, 1998; Müller et al., 2011), and for relative humidity, using the humidification

[Title Page](#)

[Abstract](#)

[Introduction](#)

[Conclusions](#)

[References](#)

[Tables](#)

[Figures](#)

◀

▶

◀

▶

[Back](#)

[Close](#)

[Full Screen / Esc](#)

[Printer-friendly Version](#)

[Interactive Discussion](#)





factors defined for Porto Velho haze in (Kotchenruther and Hobbs, 1998). A Radiance Research Particle Soot Absorption Photometer (PSAP) measured the aerosol absorption coefficient at 567 nm and standard corrections for spot size, flow rate and scattering particles were applied following Bond et al. (1999); Ogren et al. (2010) and Turnbull (2010).

Aerosol number-size distributions were measured across the 20 nm to 20  $\mu\text{m}$  range by a Scanning Mobility Particle Sizer (SMPS, 20 to 350 nm; Wang et al., 1990) and a GRIMM model 1.129 Optical Particle Counter (OPC, 0.3 to 20  $\mu\text{m}$ ; Heim et al., 2008). Note the Grimm data used in this paper is uncorrected for the minor impact of line-losses and refractive index, which is thought not to be significant for BBA below 1.0  $\mu\text{m}$ . The instrument sample is extracted through a Rosemount inlet which has been shown to measure representatively below 600 nm for aerosol in continental polluted air masses. (J. Trembath, personal communication, 2014). A Droplet Measurement Technologies Inc. (DMT) dual column Cloud Condensation Nuclei counter (CCNc) was used to measure CCN concentrations with an approximate measurement error of 7%. The operating principles are outlined in Roberts and Nenes (2005), whilst its utilisation onboard FFAM is described in Trembath (2013).

The aerosol instrumentation onboard FAAM sampled through a Rosemount inlet which, despite suffering known artefacts for larger particles, is adequate for the submicron size range of aerosols presented here (Trembath, 2013). All measured data have been converted into units of standard temperature and pressure. Further details on instruments, calibration protocols and quality assurance of data are provided in Derbyshire et al. (2014) and Morgan et al. (2014). Carbon monoxide (CO) was measured using an Aero-Laser AL5002 VUV resonance fluorescence gas analyser. The raw CO was calibrated in-flight.

From each instrument time series the influence of fresh plumes was removed, as to isolate the regional haze measurements, following the plume identification technique discussed in Darbyshire et al. (2014).

## 4.3 Model setup

For this study a modified version of WRF-Chem Version 3.4.1 has been used. A single Lambert projection domain with  $226 \times 196$  grid cells, at a horizontal spacing of 25 km, covers most of South America. 41 vertical levels are used, spaced to give greater resolution in the boundary layer. 1 km resolution global landuse data was provided by the United States Geological Survey (USGS), with vegetation maps updated for the Brazilian Legal Amazon Region with the PROVEG dataset updated for the year 2000 (Sestini et al., 2003; Freitas et al., 2011; Beck et al., 2013). Figure 1 shows the model domain with the USGS land use categorisations. The majority of the flights for this study were conducted in Rondônia State, between  $8\text{--}12^\circ\text{S}$  and  $60\text{--}65^\circ\text{W}$ , along the southern edge of the Amazon basin.

The chemistry option used was the Kinetic Pre-Processor (KPP Damian et al., 2002) compiled version of CBM-Z gas-phase chemistry (Zaveri and Peters, 1999) with 8-bin MOSAIC aerosol and aqueous chemistry (Zaveri et al., 2008). The Maxwell–Garnett mixing-rule approximation was used to calculate optical properties of the aerosol, linked with the RRTMG longwave and shortwave radiation parameterisation (Mlawer et al., 1997; Pincus et al., 2003). The physical parameterisations used for this study are summarised in Table 4. Long-term running options, for updating sea-surface temperature and other fields, were activated.

The operational, deterministic (high-resolution) 1 day forecasts of the European Centre for Medium-Range Weather Forecasts (ECMWF) <http://www.ecmwf.int/> were used to drive the meteorology. Chemical boundary conditions are taken from MACC-II. The meteorology, including satellite data assimilation, of the MACC-II assimilation system is identical (except for its lower resolution) to the operational ECMWF dataset. This ensures equivalence between the meteorological and chemical boundary conditions.

PREP-CHEM-SRC v1.4 was used to generate anthropogenic and biomass burning emission maps. Anthropogenic emissions of CO,  $\text{SO}_2$ ,  $\text{NO}_x$ ,  $\text{NH}_3$  and NMVOCs are derived from the Emissions Database for Global Atmosphere Research (EDGAR) version

[Title Page](#)[Abstract](#)[Introduction](#)[Conclusions](#)[References](#)[Tables](#)[Figures](#)[◀](#)[▶](#)[◀](#)[▶](#)[Back](#)[Close](#)[Full Screen / Esc](#)[Printer-friendly Version](#)[Interactive Discussion](#)

4.0 2005 emissions at  $0.1^\circ \times 0.1^\circ$  resolution (Olivier et al., 2002). Primary anthropogenic aerosol emissions of BC and OC at  $1^\circ \times 1^\circ$  resolution from the Goddard Chemistry Aerosol Radiation and Transport (GOCART) model databases are used (Freitas et al., 2011). Burning of residue in fields, residue and dung used as biofuels, and fuelwood and charcoal burning were included using the inventory of Yevich and Logan (2003), with the application of Andreae and Merlet (2001) emission factors, and consolidated into the anthropogenic emissions input file. Modifications to PREP-CHEM-SRC were made to convert OC into POM for all anthropogenic emissions with a factor of 1.6 (based on Turpin and Lim, 2001) and include  $\text{NH}_3$  emissions. Biogenic emissions were calculated “online” using the Model of emissions and Gases and Aerosols from Nature (MEGAN) version 2 (Guenther et al., 2006).

Fire emissions were calculated using the 3BEM emissions inventory. Two emission scenarios have been used for this study:

- Standard 3BEM emissions: default  $A_{\text{fire}} = 22.8 \text{ ha}$ ,  $S_{\text{fire}} = A_{\text{fire}} \cdot f_x = 1.3$ .
- Modified 3BEM emissions.  $A_{\text{fire}}$  and  $S_{\text{fire}}$  depend on vegetation type, as described in Table 1.  $f_x = 5$ .

Figure 2 shows horizontal maps and vertical cross-sections of the plume-risen fire emissions through  $9^\circ \text{S}$  for the two scenarios. The four panels on the left are for Phase I, while the four right panels are for Phase II. The horizontal distribution is similar for both scenarios. There is a significant reduction in average emissions in the second phase of the campaign, along with a relative shift of emissions eastwards to drier, cerrado regions. This shift in distribution is largely controlled by change in number and location of fire-pixels.

The vertical profiles of emissions show much greater differences between the two scenarios. The cerrado fires, predominantly east of  $50^\circ \text{W}$ , have peak injection heights just above 4 km in both emissions scenarios, around the same height or just above as the daytime boundary layer. The western fires, which are predominantly tropical forest biomes, peak between 5 and 12 km in the standard 3BEM scenario, and 3–6 km in

The injection height shows a strong diurnal cycle, reflecting the cycle of fire activity which follows a fixed parameterisation in this study. Flaming emissions are injected just above ground at night and the early morning/late evening. Over the course of 10 the day, as the atmosphere becomes more unstable, the injection height for each fire will typically make a discontinuous “jump” into the higher levels of the atmosphere as and when the convection is triggered within the parameterisation. The time and 15 height of this “jump” varies from day-to-day, depending on the ambient meteorological conditions, and is highly non-linear. The behaviour of the diurnal cycle in emissions and injection height can be observed in the video of model CO over the campaign period rendered using VAPoR (Clyne et al., 2007) included in the Supplement.

The scenarios were run from 1 September to 1 October 2012, encompassing all the flights of interest. Between 1 September 2012 and 11 September the model was run with meteorological nudging. From 11 September to 1 October, meteorological fields were reset from the ECMWF data every two or three days. Between 1 and 14 September the model outputted data 3 hourly, with the first three days ignored as spin-up. This period was needed to both give time for spin-up and because the aerosol loadings were higher at this time, providing interesting comparisons against satellite and ground-based measurements. From 14 September, model data was outputted hourly to give higher temporal resolution when comparing with flight data.

Title Page

Abstract      Introduction

Conclusions      References

Tables      Figures

◀      ▶

◀      ▶

Back      Close

Full Screen / Esc

Printer-friendly Version

Interactive Discussion



## 5 Results and analysis

The purpose of this study is to characterise the aerosol population and compare with measurements. The aim is to develop as accurate a picture as possible of the horizontal and vertical distribution, size distribution and composition.

5 Prior to investigating the aerosol carried by the model, we will establish that it represents the meteorological fields with a reasonable level of accuracy. Aerosol loss processes are dominated by wet deposition, and the injection height of the flaming emissions will depend partly on the vertical profile of the atmosphere and wind speed in the column. We will then proceed into more in-depth characterisation of the aerosol, 10 firstly over the whole period of the campaign against remote satellite measurements and long term AERONET sites, then with more detailed in-situ measurements from the SAMBBA aircraft campaign.

### 5.1 Verification of meteorology and stability profile of atmospheric column

Figure 3 shows maps of average precipitation over the two phases of the campaign. 15 The two panels on the left are derived from the TRMM 3B42 product of 3 hourly gridded precipitation at  $0.25^\circ \times 0.25^\circ$  resolution (Huffman et al., 2001, 2013). The broad trends and magnitude of precipitation are well represented in the model. The average daily precipitation over South America in Phase I is significantly lower than in Phase II and largely concentrated in the North-West. In Phase II, the average rate is much higher 20 and the precipitation spreads much further into the central states. However, some fine detail is missed in the model and the precipitation does not spread as far east as the TRMM data suggests. For example, there are several instances of storms in phase II between 45 and  $50^\circ$  W not reproduced in the model.

Precipitation trends over the course of the campaign had a strong impact on the BBA 25 concentrations in the western regions, both because increased precipitation reduced the number of fires and increased the level of wet deposition in the biomass burning regions. Phase I was characterised by the accumulation of regional haze, with some

GMDD

7, 6061–6131, 2014

---

## SAMBBA WRF-Chem setup

S. Archer-Nicholls et al.

---

[Title Page](#)

[Abstract](#)

[Introduction](#)

[Conclusions](#)

[References](#)

[Tables](#)

[Figures](#)

◀

▶

◀

▶

[Back](#)

[Close](#)

[Full Screen / Esc](#)

[Printer-friendly Version](#)

[Interactive Discussion](#)



localised removal events. Widespread precipitation throughout Phase II largely washed out the accumulated haze, but continued burning maintained a polluted haze, albeit relatively clean compared to Phase I. Throughout, conditions remained dry in the Eastern states.

5 Drop-sondes were used during the SAMBBA flights to measure temperature, moisture content and wind speed in the atmospheric column. Skew-T plots from drop-sondes from four flights are compared with model data in Fig. 4. Skew-T plots for all other drop-sondes made during the SAMBBA campaign can be seen in the Supplement. The model generally represents the coarse structure and wind direction of  
10 the column well. However it fails to reproduce some of the fine detail. This is unsurprising given the relatively coarse vertical and horizontal resolution of the model. The fit for the temperature profile is better than for the dewpoint profile, with several examples of stratification in the dewpoint profile observed in the flights not seen in the model. For example between 850 and 700 hPa in flight B737 (Fig. 4C), the model significantly overestimates the moisture content of the atmosphere. It was observed on the  
15 SAMBBA flights that these dew point inversions would cap aerosol transport, forming distinct layers. This is a phenomena we are unlikely to reproduce in the model. The top of the modelled boundary layer, inferred from the inversion in the temperature profile, is generally close to that observed in the measurements, but not as clearly defined or  
20 strong.

## 5.2 Horizontal distribution and optical properties of aerosol – comparison with remote sensing data

25 Figure 5 shows averaged aerosol optical depth (AOD) at 550 nm over the two phases of the campaign. The panels on the left show AOD from combined MODIS and TERRA satellites, whilst the centre and right panels show AOD from model runs using standard 3BEM emissions and the modified emission setup respectively.

Phase I is characterised by a build up of BBA, forming a large regional haze with high AOD over much of central South America. The magnitude of the AOD is well captured

[Title Page](#)

[Abstract](#)

[Introduction](#)

[Conclusions](#)

[References](#)

[Tables](#)

[Figures](#)

◀

▶

◀

▶

[Back](#)

[Close](#)

[Full Screen / Esc](#)

[Printer-friendly Version](#)

[Interactive Discussion](#)



**SAMBBA WRF-Chem setup**

S. Archer-Nicholls et al.

[Title Page](#)[Abstract](#)[Introduction](#)[Conclusions](#)[References](#)[Tables](#)[Figures](#)[◀](#)[▶](#)[◀](#)[▶](#)[Back](#)[Close](#)[Full Screen / Esc](#)[Printer-friendly Version](#)[Interactive Discussion](#)

in the model, and is closest to that observed by the satellites in the modified emission scenario. However, the distribution is displaced: the highest AODs observed by the satellites are in central Mato Grosso state, around 55° W and 15° S, while in both model runs it is in Rondônia state further to the north west, particularly about a cluster of fires

5 at 64° W and 10° S. During Phase I, both model runs also show a significant proportion of BBA are transported west. This is due to a combination of both a greater proportion of the emissions originating in western states/forest fires and a greater proportion of the aerosol being in the upper levels of the troposphere. Figure 4a and b show easterly winds in the free troposphere and northerlies in the boundary layer over these flights.

10 During Phase II, both model and satellite data show reduced AOD over much of the domain. The satellite measurements show a large reduction in BBA over Rondônia, but significant AOD in the North-Eastern states where most fires are cerrado. In the model runs, there is an eastward shift compared to Phase I, particularly in the modified emission scenario, but AOD in the eastern regions is still lower than that observed by the satellites. In addition there are significant regions of high modeled AOD in the 15 western states not observed by the satellites.

Figure 6 shows the timeseries of AOD at 550 nm measured at 4 of the AERONET sites marked in Fig. 5, including measurements from overpasses of the MODIS AQUA and TERRA satellites. The panels on the left show the standard 3BEM emissions and 20 the panels on the right are for modified emissions. There is little difference in AOD simulated at these sites between the two emission scenarios. With the exception on the Cuiaba site, the model replicates the build up of aerosol and AODs in the first half of the campaign well (although it should be noted that  $f_x$  was tuned to be able to represent the magnitude of AODs in this part of the campaign). The Cuiaba site is likely 25 too low in the model because this region is more dominated by cerrado fires, whereas the other sites have a greater proportion of forest fires nearby.

In Phase II of the campaign, the model runs overestimate the AOD over every Aeronet site evaluated against. It proved to be a challenge to find a suitable scaling factor to enable a large enough build up of AOD in the first half of the campaign without

“overshooting” in phase II. This may be due to the model not washing out aerosol as efficiently as it should, the emissions not decreasing in intensity enough in the second half, or a combination of these factors.

### 5.3 Comparisons with in-situ aircraft measurements

#### 5.3.1 Vertical distribution of CO and BBA

In this section of the paper, we will be comparing model results with in-situ measurements of aerosol and aerosol optical properties from flights conducted during the SAMBBA campaign. The remainder of the analysis will focus on four flights as case studies: B731, B734, B739 and B742 on 14, 18, 23 and 27 September 2012 respectively. The flight details are summarised in Table 5. These flights were selected as they extensively sampled the regional haze across the range of environments and meteorological conditions encountered during the campaign, with near complete instrument coverage. Flights B731, B734, B739 sampled the regional haze in Rondônia state, characterised by cleared and pristine forest, whilst B742 sampled over Tocantins state in the Cerrado (savannah-like) environment. All aerosol data from the model has been summed over bins where  $D_p$  is  $< 1\mu\text{m}$  (defined as all bins 1–4 and 67.8 % of bin 5) and converted to standard temperature and pressure units ( $\mu\text{g sm}^{-3}$ ) for comparison with submicron flight measurements.

The paths of the flights used in this study are shown in Fig. 7. Following a profile ascent out of the host airport (Porto Velho for B731, B734 and B739, Palmas for B742), the aircraft travelled to the region of interest at high altitude (7–8 km a.s.l.), before descending to near surface via a stack of straight and level runs at altitudes above and within the boundary layer. Flight B739 was a slight exception to this pattern, with only a brief period at high altitude, and without the straight and level runs in the stacked formation. Near surface, flights B739 and B742 sampled extensive small plumes in the area, resulting in non-uniform flight patterns. All flights then returned either at high altitude (B731, B734) or high within the boundary layer (B739, B742), before profile

[Title Page](#)[Abstract](#)[Introduction](#)[Conclusions](#)[References](#)[Tables](#)[Figures](#)[◀](#)[▶](#)[◀](#)[▶](#)[Back](#)[Close](#)[Full Screen / Esc](#)[Printer-friendly Version](#)[Interactive Discussion](#)

descent back to base. Each flight therefore had a number of profiles and straight and level runs at multiple altitudes, providing a comprehensive characterisation of the haze in the region sampled. The boxes around each of the flight paths in Fig. 7 show the area averaged over when calculating the statistics from the model when carrying out the comparisons.

Figure 8 shows vertical profiles of CO, POM and scattering coefficient at 550 nm ( $b_{\text{scat}}$ ). CO is used as a relatively inert tracer, largely unaffected by precipitation or wash-out. POM is shown and compared with AMS organics data as it makes up the dominant fraction of the total aerosol budget. Finally,  $b_{\text{scat}}$  is used to show the optical depth of the aerosol.  $b_{\text{scat}}$  is used rather than  $b_{\text{ext}}$  to avoid additional measurement uncertainty by the addition of  $b_{\text{abs}}$  (Bond et al., 2013). The dashed blue lines and shaded regions show median, interquartile and 5th–95th percentile range derived from the standard 3BEM emission scenario, while the red lines and shaded regions are for the modified emission scenario. The solid black lines show median values from the profiles conducted by each flight, while the fine grey lines show the actual flight track data. The flight data is limited by never flying above 8 km altitude. However, as a significant portion of the plume-rise emissions in the standard 3BEM case are emitted above 8 km (see Fig. 2), the profiles from the model runs are plotted up to 12 km. This measurement evaluation is an improvement over Longo et al. (2010), where the plume-risen emissions were compared against flights which did not fly above 4 km and comparisons were only made with CO.

B731 coincided with the end of a long build up of aerosol in Rondônia before it was washed out during the progression into the wet season and had some of the highest measurements of aerosol in the campaign. Both model scenarios under-predict CO and POM within the boundary layer and over-predict above the boundary layer. The flights show the majority of CO and aerosol are in the lower 2 km of the troposphere, with a steep drop off above this. Both model runs show a secondary peak in aerosol above the boundary layer, between 4–5 km in the updated emissions scenario and around 7 km using the standard 3BEM emissions. In both model runs, too

## SAMBBA WRF-Chem setup

S. Archer-Nicholls et al.

[Title Page](#)

[Abstract](#)

[Introduction](#)

[Conclusions](#)

[References](#)

[Tables](#)

[Figures](#)

◀

▶

◀

▶

[Back](#)

[Close](#)

[Full Screen / Esc](#)

[Printer-friendly Version](#)

[Interactive Discussion](#)



## SAMBBA WRF-Chem setup

S. Archer-Nicholls et al.

[Title Page](#)[Abstract](#)[Introduction](#)[Conclusions](#)[References](#)[Tables](#)[Figures](#)[◀](#)[▶](#)[◀](#)[▶](#)[Back](#)[Close](#)[Full Screen / Esc](#)[Printer-friendly Version](#)[Interactive Discussion](#)

large a proportion of the emissions are being emitted above the boundary layer. The same elevated peak can be observed in  $b_{\text{scat}}$ , although it decreases faster above the boundary layer than POM. This is because POM is in units at standard temperature and pressure and independent of altitude, while  $b_{\text{scat}}$  is related to the absolute density of particles and decreases exponentially with altitude.  $b_{\text{scat}}$  is therefore dominated by aerosol in the boundary layer in both flight and model.

By the time of flight B734, significant precipitation had occurred over Rondônia, reducing the aerosol loadings in both model and measurements. The flight is also sampling a different region of Rondônia. CO in the boundary layer is also lower, implying reduced fire emissions. Below 4 km, flight CO and POM are similar to the modified emissions scenario. Above 4 km, CO remains elevated in both measurement and model. POM sharply decreases in the flight data, while in the model it is clear the POM has been emitted at the same height as the CO and follows a similar profile. The lack of observed POM at the same altitude as CO implies either the wash-out processes are not being well represented in the model, both CO and POM are being emitted at altitude in an unrealistic fashion with less of a negative impact on CO or the flight is measuring a source of CO that does not have much associated POM.

Flight B739 was conducted at the start of Phase II, by which time the majority of accumulated aerosol in the western states had been washed out. During this flight, there were large stratocumulus clouds and significant convection over the region. The increased soil moisture after previous days precipitation meant many of the fires were smouldering. Given the limitations of the model setup, we would expect this flight to be the most challenging of the case studies for the model. High concentrations of CO and slightly elevated POM in the lowest km of the boundary layer are observed, but these fresh emissions have not become well mixed at the time of flights. Aside from that, the measured atmosphere is relatively clean compared to the earlier flights. The standard 3BEM emission scenarios is close to the measurements for CO, at least up to 6 km altitude, whereas the modified emission scenario has too much CO. However, both model scenarios overpredict POM in and above the boundary layer. The elevated

peak in POM and CO in the model is much higher during this period, especially in the standard 3BEM case where it is above where the flights can observe. While the existence of this layer cannot be ruled out, from the good agreement between aircraft and satellite derived AOD it can be inferred that the magnitude of aerosol loadings are 5 unlikely (see Derbyshire et al., 2014). This elevated peak results from a combination of high plume-risen injected emissions and convective transport.

Flight B742 was carried out in the eastern Tocantins state. This region is dominated by cerrado fires. It is clear that the magnitude of emissions are too low in the region. CO, POM and  $b_{\text{scat}}$  are higher in the modified emissions scenario, but still approximately 10 50 % below measured. However, the shape of the vertical profile is well represented, with flights and both model scenarios showing aerosol and CO well mixed within the boundary layer, and little above it. The lower carbon density of the cerrado biome to tropical forests results in less intense fires, with the injection height is rarely much higher than the top of the boundary layer.

15 Overall, flight B734 shows the closest correspondence between the measurements and model data of the case studies. The modified emissions do produce on average a more reasonable injection height to represent flaming emissions. However, there is still a strong bias towards overestimating the injection height, particularly over tropical forest biomes. This is most apparent in POM, while modelled CO may be similar to 20 flights even where POM diverges.  $b_{\text{scat}}$  decreases exponentially with altitude, meaning the high altitude layers are optically thinner than those in the boundary layer. However, this may still be a significant divergence from reality, given the negligible measured  $b_{\text{scat}}$  at these heights.

### 5.3.2 Composition, optical properties and size distribution of aerosol

25 Box and whisker plots of BC, POM : BC ratio and single scattering albedo ( $\omega_0$ ) for the straight level runs below 3 km of the atmosphere are shown in Fig. 9. During flight B731, the SP2 was not functional for much of the flight and had little crossover with when the AMS was working, and so has been left out of this section of the analysis, although  $\omega_0$

[Title Page](#)[Abstract](#)[Introduction](#)[Conclusions](#)[References](#)[Tables](#)[Figures](#)[◀](#)[▶](#)[◀](#)[▶](#)[Back](#)[Close](#)[Full Screen / Esc](#)[Printer-friendly Version](#)[Interactive Discussion](#)

measurements for B731 have been included in the Supplement. Model data is from the modified emissions scenario, extracted along the flight path by finding the  $x$ - $y$  grid point closest to the flight measurement, then linearly interpolating in the vertical and time to the altitude and time of reading. There was little difference in composition between the two scenarios.

The western flights show a higher POM : BC ratio on average compared to the Eastern flight B742. In both western flights, the modelled POM : BC ratio is much lower than measured, due to the increased loadings of BC. The modelled POM : BC ratio is consistently between 9 and 11, slightly higher on B739 and lower in B742. The median measured ratio for B734 is 14.5 and for B739 it is 17.6. B739 is likely higher due to the increased proportion of smouldering fires post precipitation, which tend to have higher POM : BC ratio. In the eastern flight B742, the median POM : BC ratio is 9.1, similar to the modelled, although the range is still larger. The lower POM : BC ratio in flight B742 is likely due to the higher proportion of cerrado fires.

The POM : BC ratio shows a lot more variability in the flight data compared to the model. The variation is likely due to a combination of varying emission factors (EF) due to fuel type, flaming temperature, burning efficiency, and other factors (Jolley et al., 2012); and SOA formation (Jimenez et al., 2009). The model emissions do not vary in composition to the same extent, due to limited measurements driving the Andreae and Merlet (2001) EF, and no SOA formation is represented in the MOSAIC mechanism. Some recent measurements, such as Jolley et al. (2012), suggest that, unlike urban plumes, there is little net SOA formation during the ageing of BB plumes, supporting the primary OC assumption in heavily BB influenced regions. However, other studies, such as Vakkari et al. (2014), suggest growth by SOA condensation in the first few hours of plume ageing is a significant factor in determining BBA composition.

Modelled  $\omega_0$  is largely controlled by the ratio of BC to other aerosol components. In flights B734 and B739, the flight average is similar to modelled  $\omega_0$ , if slightly higher on average. B739 shows a much greater degree of variability, with an IQR of 0.86–0.95. However, it should be noted that the PSAP instrument had only partial coverage during

[Title Page](#)[Abstract](#)[Introduction](#)[Conclusions](#)[References](#)[Tables](#)[Figures](#)[◀](#)[▶](#)[◀](#)[▶](#)[Back](#)[Close](#)[Full Screen / Esc](#)[Printer-friendly Version](#)[Interactive Discussion](#)

this flight, which may be skewing some of the data. However, while the POM : BC ratio is always lower in the model,  $\omega_0$  is often lower in the measurements. Given the low modelled POM : BC ratio, the model should be underestimating  $\omega_0$  by a similar margin; i.e. it is getting  $\omega_0$  right for the wrong reasons. In contrast, flight B742 has a similar

5 POM : BC ratio between flight and model but significantly lower  $\omega_0$  (the model is getting it wrong for the right reasons). The implication is that there are properties of the aerosol affecting how it absorbs radiation not being captured in the model. The mixing rule (in this case Maxwell-Garnett) may be under-predicting the absorption amplification of the other aerosol components and/or the organic portion of the aerosol should be slightly 10 absorbing in the visible spectrum (“brown” carbon). Explicit resolution of the aerosol mixing state, as is done by Matsui et al. (2013) could also improve results.

Figure 10 shows the CCN concentration and size distribution of aerosol from flights B734 and B742 compared with the modified emission scenario. Data was extracted from the model along the flight path. In both flights, the peak in the size distribution is 15 the same (within error), showing the studies the modelled distribution is based on are representative of regional BBA. However, the modeled distribution is too wide, with too much aerosol in the larger bins between 1 and 5  $\mu\text{m}$  and too little in the accumulation mode. This implies that there is too much emitted coarse mode BBA, there is another source of coarse aerosol (e.g. dust) in the model not observed in the flight, too much 20 coarse aerosol is being transported up to flight height, or the process of larger BBA particles being preferentially removed by precipitation (as Taylor et al., 2014, show with Canadian fires) is not being well captured in the model. However, it should be noted that the GRIMM data has some minor uncertainties attributed to it due to line-losses and refractive index. The results presented should be seen as a lower limit. 25 Further sensitivity work is needed to test which of these factors are more important. The model represents the spread of CCN well in flight B734, with the measured CCN at 0.14 % supersaturation ( $\text{CCN}_{0.14}$ ) in between the modeled  $\text{CCN}_{0.1}$  and  $\text{CCN}_{0.2}$  values. The model also underestimates CCN concentrations over flight B742, in line with the under-prediction of aerosol loadings over the eastern regions.

## SAMBBA WRF-Chem setup

S. Archer-Nicholls et al.

[Title Page](#)[Abstract](#)[Introduction](#)[Conclusions](#)[References](#)[Tables](#)[Figures](#)[◀](#)[▶](#)[◀](#)[▶](#)[Back](#)[Close](#)[Full Screen / Esc](#)[Printer-friendly Version](#)[Interactive Discussion](#)

## 6 Conclusions

We have modified the online couple regional model WRF-Chem to use 3BEM emissions and plume-rise parameterisation with the MOSAIC sectional aerosol and CBM-Z gas phase chemistry mechanisms. The default values of both active fire size and burned area given in PREP-CHEM-SRC are 22.8 ha (Longo et al., 2010). Using these values it was found that the injection height would often be biased high. Given the downward trend in fire sizes in Brazil from 2000, emissions suitable for the 2012 Brazilian biomass burning season have been developed. Estimates are based on FRP measurements over the 2012 South American biomass burning season, with different values used for different biomes. In the modified inventory, burned area and active fire size are treated independently, where the burned area is used to calculate the emitted mass and active fire size to calculate the injection height of the plume-rise parameterisation. Results from the model simulations have been compared against in-situ measurements from the SAMBBA flight campaign.

In many modelling studies and emission products, an enhancement factor ( $f_x$ ) is required to scale fire emissions to produce reasonable AODs (e.g. Wu et al., 2011a; Kaiser et al., 2012; Tosca et al., 2013). The need for  $f_x$  highlights the many uncertainties in calculating biomass burning emissions (Ichoku et al., 2012). Factors causing this include underestimating the biomass density or burn fraction, satellite products missing some fires, due to overpass times, cloud cover, fires being too small to detect, or multiple fires within the same  $1 \text{ km}^2$  being assigned a single fire pixel. In this study, we found when updating the estimated burned area for 2012 values, the total emitted mass was significantly smaller. We therefore increased the emission amplification factor  $f_x$  from 1.3 to 5 in order to produce reasonable AODs within the model. The implication is that using the standard 3BEM emission product the modelled AOD was reasonable, but only because the burned area was larger than the 2012 season average. Using our best estimate of burned area required a scaling of emissions to compensate.

## SAMBBA WRF-Chem setup

S. Archer-Nicholls et al.

[Title Page](#)

[Abstract](#)

[Introduction](#)

[Conclusions](#)

[References](#)

[Tables](#)

[Figures](#)

◀

▶

◀

▶

[Back](#)

[Close](#)

[Full Screen / Esc](#)

[Printer-friendly Version](#)

[Interactive Discussion](#)



In the western regions over the first half of the campaign, modelled AODs compared well to satellite measurements. However, in the second half of the campaign the model consistently overestimate AODs in the western regions. Over Eastern cerrado regions, the model underestimated AOD over the whole campaign. There are several factors that may explain these observations. We used an average burned area across the whole season, which does not vary if fires were smaller and less vigorous in the second phase of the campaign. Distribution of fire size is heavily skewed to mostly small fires with a few massive ones, something not represented using a mean fire size. Observations on the SAMBBA flights were that in some regions there were more than one fire per  $\text{km}^2$ , particularly in the eastern cerrado burning states. Randerson et al. (2012) estimate some 35 % of fire emissions are missed globally due to lack of detection of small fires, with this factor being larger in some regions. The emissions inventory of Yovich and Logan (2003) has been used in this study to account for small scale biofuel and agricultural burnings. However, the inventory provides annual averages for emissions which are known to show large seasonal variability (Duncan, 2003). Adding a function to control the seasonal variation in these emissions would increase their contribution to the aerosol loadings in the dry season, which should provide better estimates, particularly in rural agricultural areas such the eastern cerrado states.

Over the western flights, which were dominated by tropical forest fires (and pasture burnings), there was too much emitted mass at high altitude in both model scenarios. With fire size significantly smaller in the modified emission scenario, the injection height was typically 2–3 km lower, but still approximately 2 km above the boundary layer. Val Martin et al. (2010b) show that the majority of tropical forest fires inject into the boundary layer, with only a few large outliers penetrating higher. The distribution of fire size is positively skewed, with the majority of fires being small ( $\ll 5 \text{ ha}$ ) and only a few large fires (some 50 ha or larger). Using a simple average does not represent this distribution. A better probabilistic representation may be needed to represent the size distribution of fires in the model to account for this.

<a href="#">Title Page</a>	
<a href="#">Abstract</a>	<a href="#">Introduction</a>
<a href="#">Conclusions</a>	<a href="#">References</a>
<a href="#">Tables</a>	<a href="#">Figures</a>
<a href="#">◀</a>	<a href="#">▶</a>
<a href="#">◀</a>	<a href="#">▶</a>
<a href="#">Back</a>	<a href="#">Close</a>
<a href="#">Full Screen / Esc</a>	
<a href="#">Printer-friendly Version</a>	
<a href="#">Interactive Discussion</a>	



The vertical stability in the atmospheric column from the model was compared with dropsonde measurements from the flight. The coarse structure was well captured but much of the fine detail was not represented in the model. The model failed to reproduce the temperature and dewpoint inversions at the top of the boundary layer, likely due to

5 vertical resolution issues and limitations of the PBL parameterisation. The stability profile from the parent model is used to define the column of the plume rise parameterisation. Without a clearly defined stable layer in the temperature profile, it is unsurprising the parameterisation often penetrates the boundary layer. Forcing a small temperature inversion at the PBL top in the plume-rise parameterisation may be needed to improve  
10 its accuracy.

The vertical distribution of carbon monoxide (CO), particulate organic matter (POM) and scattering coefficient ( $b_{\text{scat}}$ ) were compared between model runs and flight measurements. The modelled CO vertical profile was reasonably well represented, as seen in previous studies (Freitas et al., 2007, 2009; Longo et al., 2010). However, there were  
15 regions of elevated aerosol layers in the model not observed in flight measurements. Aerosol has many more loss processes than CO, particularly through wash-out. Andreae et al. (2001) show convective transport of tropical BBA is important for forming aerosol layers at high altitude. However, only around 5–20 % of accumulation mode aerosol is retained during transport; the rest is washed out. The plume-rise parameterisation transports 100 % of flaming emissions when convection is triggered. Accounting  
20 for the aerosol loss processes attributed to convection during plume-rise may be needed to better represent the aerosol profile.

The model failed to represent the same variation in aerosol composition and  $\omega_0$  observed in the flights. This composition in the model is driven by the Andreae and  
25 Merlet (2001) EF. Akagi et al. (2011) have reviewed many more recent studies to provide newer estimates. The OC : BC ratio for savannah has remained the same at 7.08. However, the estimated tropical forest EF increased from 7.88 to 9.05, approximately 15 % higher. Using updated EF would bring the model closer to typical POM : BC ratios in the western flights. Work is underway to update the PREP-CHEM-SRC to the

[Title Page](#)[Abstract](#)[Introduction](#)[Conclusions](#)[References](#)[Tables](#)[Figures](#)[◀](#)[▶](#)[◀](#)[▶](#)[Back](#)[Close](#)[Full Screen / Esc](#)[Printer-friendly Version](#)[Interactive Discussion](#)

EF of Akagi et al. (2011). Representing flight B739 will still be a challenge however, given the impact of precipitation on fire conditions. Using different EF for smouldering and flaming emissions, with flaming and smouldering fraction varying dynamically with soil moisture, may be able to represent this variation of emissions. More detailed

5 measurements need to be collected and reviewed to develop an emissions inventory with this flexibility. It should also be noted that comparisons are between primary organic matter from the model with total organic matter from measurements (including contribution from SOA). Developments including SOA treatment in WRF-Chem, such as using the VBS (Shrivastava et al., 2011, 2013), could be needed to represent the  
10 observed variation in composition.

Modeled  $\omega_0$  was often too high when the POM:BC ratio was approximately correct, and close to measured when POM:BC ratio was too low. Improving the aerosol composition in the model is needed before we can evaluate the  $\omega_0$ . However, this indicates failure of the model to accurately predict the aerosol optical properties from the  
15 composition. The behaviour of the optical calculations can be tested by initialising the optical properties subroutine with SAMBBA flight measurements, showing how much of the discrepancy is due to inadequacies in the calculations (Barnard et al., 2010). The model may be underestimating the enhancement factor of BC and a better mixing-rule is needed (such as shell-core), or explicit modeling of the BC mixing state (Matsui  
20 et al., 2013). Some SW absorption due to the “brown carbon” components of organic aerosol is also likely needed (Lack et al., 2012, 2013; Saleh et al., 2014). The discrepancies highlight the need to capture the full mixing state, including both SOA and POA, as well as condensable inorganic vapours, to represent aerosol optical properties.

The model represented size distribution peak location well in flights B734 and B742.  
25 CCN concentrations correspond well over the western flight B734, with CCN<sub>0.2</sub> between 900 and 1100  $\text{scm}^{-3}$  within the boundary layer. Over the eastern flight, the model underpredicted CCN concentration. However, the low CCN concentrations are in line with the low aerosol loadings over this flight and period.

---

**SAMBBA WRF-Chem setup****S. Archer-Nicholls et al.**

---

[Title Page](#)[Abstract](#)[Introduction](#)[Conclusions](#)[References](#)[Tables](#)[Figures](#)[◀](#)[▶](#)[◀](#)[▶](#)[Back](#)[Close](#)[Full Screen / Esc](#)[Printer-friendly Version](#)[Interactive Discussion](#)

SAMBBA WRF-Chem  
setup

S. Archer-Nicholls et al.

Title Page

Abstract

Introduction

Conclusions

References

Tables

Figures

◀

▶

◀

▶

Back

Close

Full Screen / Esc

Printer-friendly Version

Interactive Discussion



## References

Abdul-razzak, H. and Ghan, S. J.: A parameterization of aerosol activation 3. Sectional representation, *J. Geophys. Res.*, 107, 4026, doi:10.1029/2001JD000483, 2002. 6064, 6120

Ackermann, I. J., Hass, H., Memmesheimer, M., Ebel, A., Binkowski, F. S., and Shankar, U.:  
5 Modal aerosol dynamics model for Europe: development and first applications, *Atmos. Environ.*, 32, 2981–2999, 1998. 6066

Ackerman, T. P. and Toon, O. B.: Absorption of visible radiation in atmosphere containing mixtures of absorbing and nonabsorbing particles, *Appl. Optics*, 21, 758, doi:10.1364/AO.21.000758, 1982. 6069

10 Akagi, S. K., Yokelson, R. J., Wiedinmyer, C., Alvarado, M. J., Reid, J. S., Karl, T., Crounse, J. D., and Wennberg, P. O.: Emission factors for open and domestic biomass burning for use in atmospheric models, *Atmos. Chem. Phys.*, 11, 4039–4072, doi:10.5194/acp-11-4039-2011, 2011. 6098, 6099

15 Andela, N., Kaiser, J. W., Heil, A., van Leeuwen, T. T., Wooster, M. J., van der Werf, G. R., Remy, S., and Schultz, M. G.: Assessment of the Global Fire Assimilation System (GFASv1), Tech. Memo. 702, European Centre for Medium-range Weather Forecasts (ECMWF), Reading, UK, 2013. 6065

20 Anderson, T. L. and Ogren, J. A.: Determining aerosol radiative properties using the TSI 3563 integrating nephelometer, *Aerosol Sci. Tech.*, 29, 57–69, doi:10.1080/02786829808965551, 1998. 6082

Anderson, T. L., Covert, D. S., Marshall, S. F., Laucks, M. L., Charlson, R. J., Waggoner, A. P.,  
25 Ogren, J. A., Caldow, R., Holm, R. L., Quant, F. R., Sem, G. J., Wiedensohler, A., Ahlquist, N. A., and Bates, T. S.: Performance Characteristics of a High-Sensitivity, Three-Wavelength, Total Scatter/Backscatter Nephelometer, *J. Atmos. Ocean. Tech.*, 13, 967–986, doi:10.1175/1520-0426(1996)013<0967:PCOAH>2.0.CO;2, 1996. 6082, 6121

30 Andreae, M. O. and Merlet, P.: Emission of trace gases and aerosols from biomass burning, *Global Biogeochem. Cy.*, 15, 955–966, 2001. 6071, 6077, 6085, 6094, 6098

Andreae, M. O., Artaxo, P., Fischer, H., Freitas, S. R., Grgoire, J.-M., Hansel, A., Hoor, P., Kormann, R., Krejci, R., Lange, L., Lelieveld, J., Lindinger, W., Longo, K., Peters, W., de Reus, M., Scheeren, B., Silva Dias, M. A. F., Strm, J., van Velthoven, P. F. J., and Williams, J.: Transport of biomass burning smoke to the upper troposphere by deep convection in the equatorial region, *Geophys. Res. Lett.*, 28, 951–954, doi:10.1029/2000GL012391, 2001. 6065, 6098

## SAMBBA WRF-Chem setup

S. Archer-Nicholls et al.

[Title Page](#)

[Abstract](#)

[Introduction](#)

[Conclusions](#)

[References](#)

[Tables](#)

[Figures](#)

◀

▶

◀

▶

[Back](#)

[Close](#)

[Full Screen / Esc](#)

[Printer-friendly Version](#)

[Interactive Discussion](#)



Andreae, M. O., Rosenfeld, D., Artaxo, P., Costa, A. A., Frank, G. P., Longo, K. M., and Silva-Dias, M. A. F.: Smoking rain clouds over the Amazon, *Science*, 303, 1337–1342, doi:10.1126/science.1092779, 2004. 6064, 6072

Arai, E., Shimabukuro, Y. E., Pereira, G., and Vijaykumar, N. L.: A multi-resolution multi-temporal technique for detecting and mapping deforestation in the Brazilian Amazon rain-forest, *Remote Sens. Environ.*, 3, 1943–1956, doi:10.3390/rs3091943, 2011. 6075

Artaxo, P., Rizzo, L. V., Brito, J. F., Barbosa, H. M. J., Arana, A., Sena, E. T., Cirino, G. G., Bastos, W., Martin, S. T., and Andreae, M. O.: Atmospheric aerosols in Amazonia and land use change: from natural biogenic to biomass burning conditions, *Faraday Discuss.*, 165, 203, doi:10.1039/c3fd00052d, 2013. 6075

Bahreini, R., Ervens, B., Middlebrook, A. M., Warneke, C., de Gouw, J. A., DeCarlo, P. F., Jimenez, J. L., Brock, C. A., Neuman, J. a., Ryerson, T. B., Stark, H., Atlas, E., Brioude, J., Fried, A., Holloway, J. S., Peischl, J., Richter, D., Walega, J., Weibring, P., Wollny, A. G., and Fehsenfeld, F. C.: Organic aerosol formation in urban and industrial plumes near Houston and Dallas, Texas, *J. Geophys. Res.*, 114, D00F16, doi:10.1029/2008JD011493, 2009. 6082

Baklanov, A., Schlünzen, K., Suppan, P., Baldasano, J., Brunner, D., Aksoyoglu, S., Carmichael, G., Douros, J., Flemming, J., Forkel, R., Galmarini, S., Gauss, M., Grell, G., Hirtl, M., Joffre, S., Jorba, O., Kaas, E., Kaasik, M., Kallos, G., Kong, X., Korsholm, U., Kurganskiy, A., Kushta, J., Lohmann, U., Mahura, A., Manders-Groot, A., Maurizi, A., Moussiopoulos, N., Rao, S. T., Savage, N., Seigneur, C., Sokhi, R. S., Solazzo, E., Solomos, S., Sørensen, B., Tsegas, G., Vignati, E., Vogel, B., and Zhang, Y.: Online coupled regional meteorology chemistry models in Europe: current status and prospects, *Atmos. Chem. Phys.*, 14, 317–398, doi:10.5194/acp-14-317-2014, 2014. 6068

Ban-Weiss, G. A., Cao, L., Bala, G., and Caldeira, K.: Dependence of climate forcing and response on the altitude of black carbon aerosols, *Clim. Dynam.*, 38, 897–911, doi:10.1007/s00382-011-1052-y, 2011. 6067

Barnard, J. C., Fast, J. D., Paredes-Miranda, G., Arnott, W. P., and Laskin, A.: Technical Note: Evaluation of the WRF-Chem “Aerosol Chemical to Aerosol Optical Properties” Module using data from the MILAGRO campaign, *Atmos. Chem. Phys.*, 10, 7325–7340, doi:10.5194/acp-10-7325-2010, 2010. 6069, 6070, 6099

Baumgardner, D., Kok, G., and Raga, G.: Warming of the Arctic lower stratosphere by light absorbing particles, *Geophys. Res. Lett.*, 31, L06117, doi:10.1029/2003GL018883, 2004. 6082, 6121

## SAMBBA WRF-Chem setup

S. Archer-Nicholls et al.

[Title Page](#)

[Abstract](#)

[Introduction](#)

[Conclusions](#)

[References](#)

[Tables](#)

[Figures](#)

◀

▶

◀

▶

[Back](#)

[Close](#)

[Full Screen / Esc](#)

[Printer-friendly Version](#)

[Interactive Discussion](#)



Beck, V., Gerbig, C., Koch, T., Bela, M. M., Longo, K. M., Freitas, S. R., Kaplan, J. O., Prigent, C., Bergamaschi, P., and Heimann, M.: WRF-Chem simulations in the Amazon region during wet and dry season transitions: evaluation of methane models and wetland inundation maps, *Atmos. Chem. Phys.*, 13, 7961–7982, doi:10.5194/acp-13-7961-2013, 2013. 6084

5 Bela, M. M., Longo, K. M., Freitas, S. R., Moreira, D. S., Beck, V., Wofsy, S. C., Gerbig, C., Wiedemann, K., Andreae, M. O., and Artaxo, P.: Ozone production and transport over the Amazon Basin during the dry-to-wet and wet-to-dry transition seasons, *Atmos. Chem. Phys. Discuss.*, 14, 14005–14070, doi:10.5194/acpd-14-14005-2014, 2014. 6066

10 Benedetti, A., Morcrette, J.-J., Boucher, O., Dethof, A., Engelen, R. J., Fisher, M., Flentje, H., Huneeus, N., Jones, L., Kaiser, J. W., Kinne, S., Mangold, A., Razinger, M., Simmons, A. J., and Suttie, M.: Aerosol analysis and forecast in the European Centre for Medium-Range Weather Forecasts Integrated Forecast System: 2. Data assimilation, *J. Geophys. Res.*, 114, D13205, doi:10.1029/2008JD011115, 2009. 6079

15 Brito, J., Rizzo, L. V., Morgan, W. T., Coe, H., Johnson, B., Haywood, J., Longo, K., Freitas, S., Andreae, M. O., and Artaxo, P.: Ground based aerosol characterization during the South American Biomass Burning Analysis (SAMBBA) field experiment, *Atmos. Chem. Phys. Discuss.*, 14, 12279–12322, doi:10.5194/acpd-14-12279-2014, 2014. 6079, 6081

20 Bond, T. C. and Bergstrom, R. W.: Light absorption by carbonaceous particles: an investigative review, *Aerosol Sci. Tech.*, 40, 27–67, doi:10.1080/02786820500421521, 2006. 6064, 6069

25 Bond, T. C., Anderson, T. L., and Campbell, D.: Calibration and intercomparison of filter-based measurements of visible light absorption by aerosols, *Aerosol Sci. Tech.*, 30, 582–600, doi:10.1080/027868299304435, 1999. 6083, 6121

Bond, T. C., Habib, G., and Bergstrom, R. W.: Limitations in the enhancement of visible light absorption due to mixing state, *J. Geophys. Res.*, 111, D20211, doi:10.1029/2006JD007315, 2006. 6069, 6070

30 Bond, T. C., Doherty, S. J., Fahey, D. W., Forster, P. M., Berntsen, T., Deangelo, B. J., Flanner, M. G., Ghan, S., Koch, D., Kinne, S., Kondo, Y., Quinn, P. K., Sarofim, M. C., Schultz, M. G., Schulz, M., Zhang, H., Zhang, S., Bellouin, N., Guttikunda, S. K., Hopke, P. K., Jacobson, M. Z., Klimont, Z., Lohmann, U., Schwarz, J. P., Shindell, D., Storelvmo, T., Warren, S. G., and Zender, C. S.: Bounding the role of black carbon in the climate system: a scientific assessment, *J. Geophys. Res.-Atmos.*, 11, 1–163, 2013. 6069, 6091

Boucher, O., Randall, D., Artaxo, P., Bretherton, C., Feingold, G., Forster, P., Kerminen, V.-M., Kondo, Y., Liao, H., Lohmann, U., Rasch, P., Satheesh, S. K., Sherwood, S., Stevens, B., and

SAMBBA WRF-Chem setup

S. Archer-Nicholls et al.

[Title Page](#)

[Abstract](#)

[Introduction](#)

[Conclusions](#)

[References](#)

[Tables](#)

[Figures](#)

◀

▶

◀

▶

[Back](#)

[Close](#)

[Full Screen / Esc](#)

[Printer-friendly Version](#)

[Interactive Discussion](#)



5 Zhang, X. Y.: Clouds and aerosols, in: Climate Change 2013: the Physical Science Basis. Contribution of Working Group I to the Fifth Assessment Report of the Intergovernmental Panel on Climate Change, edited by: Stocker, T. F., Qin, D., Plattner, G.-K., Tignor, M., Allen, S. K., Boschung, J., Nauels, A., Xia, Y., Bex, V., and Midgley, P. M., Cambridge University Press, Cambridge, UK and New York, NY, USA, 2013. 6064

10 Canagaratna, M. R., Jayne, J. T., Jimenez, J. L., Allan, J. D., Alfarra, M. R., Zhang, Q., Onasch, T. B., Drewnick, F., Coe, H., Middlebrook, A., Delia, A., Williams, L. R., Trimborn, A. M., Northway, M. J., Decarlo, P. F., Kolb, C. E., Davidovits, P., and Worsnop, D. R.: Chemical and microphysical characterization of ambient aerosols with the aerodyne aerosol mass spectrometer, *Mass Spectrom. Rev.*, 26, 185–222, doi:10.1002/mas.20115, 2007. 6082, 6121

15 Clyne, J., Mininni, P., Norton, A., and Rast, M.: Interactive desktop analysis of high resolution simulations: application to turbulent plume dynamics and current sheet formation, *New J. Phys.*, 9, 301, doi:10.1088/1367-2630/9/8/301, 2007. 6086

20 Chapman, E. G., Gustafson Jr., W. I., Easter, R. C., Barnard, J. C., Ghan, S. J., Pekour, M. S., and Fast, J. D.: Coupling aerosol-cloud-radiative processes in the WRF-Chem model: Investigating the radiative impact of elevated point sources, *Atmos. Chem. Phys.*, 9, 945–964, doi:10.5194/acp-9-945-2009, 2009. 6068

25 Chin, M., Rood, R. B., Lin, S., Müller, J.-F., and Thompson, A. M.: Atmospheric sulfur cycle simulated in the global model GOCART – Model description and global properties, *J. Geophys. Res.*, 105, 24671–24687, 2000. 6066

30 Damian, V., Sandu, A., Damian, M., Potra, F., and Carmichael, G. R.: The Kinetic PreProcessor KPP – a software environment for solving chemical kinetics, *Comput. Chem. Eng.*, 26, 1567–1579, 2002. 6084

35 de Andrade Filho, V. S., Artaxo, P., Hacon, S., Nascimento do Carmo, C., and Cirino I, G.: Aerosols from biomass burning and respiratory diseases in children, Manaus, Northern Brazil, *Rev. Saude Publ.*, 47, doi:10.1590/S0034-8910.2013047004011, 2013. 6064

40 Dentener, F., Kinne, S., Bond, T., Boucher, O., Cofala, J., Generoso, S., Ginoux, P., Gong, S., Hoelzemann, J. J., Ito, A., Marelli, L., Penner, J. E., Putaud, J.-P., Textor, C., Schulz, M., van der Werf, G. R., and Wilson, J.: Emissions of primary aerosol and precursor gases in the years 2000 and 1750 prescribed data-sets for AeroCom, *Atmos. Chem. Phys.*, 6, 4321–4344, doi:10.5194/acp-6-4321-2006, 2006. 6066

[Title Page](#)[Abstract](#)[Introduction](#)[Conclusions](#)[References](#)[Tables](#)[Figures](#)[◀](#)[▶](#)[◀](#)[▶](#)[Back](#)[Close](#)[Full Screen / Esc](#)[Printer-friendly Version](#)[Interactive Discussion](#)

Dozier, J.: A method for satellite identification of surface temperature fields of subpixel resolution, *Remote Sens. Environ.*, 11, 221–229, 1981. 6071, 6075

Drewnick, F., Hings, S. S., DeCarlo, P., Jayne, J. T., Gonin, M., Fuhrer, K., Weimer, S., Jimenez, J. L., Demerjian, K. L., Borrmann, S., and Worsnop, D. R.: A New Time-of-Flight Aerosol Mass Spectrometer (TOF-AMS) instrument description and first field deployment, *Aerosol Sci. Tech.*, 39, 637–658, doi:10.1080/02786820500182040, 2005. 6082, 6121

Drewnick, F., Hings, S. S., Alfarra, M. R., Prevot, A. S. H., and Borrmann, S.: Aerosol quantification with the Aerodyne Aerosol Mass Spectrometer: detection limits and ionizer background effects, *Atmos. Meas. Tech.*, 2, 33–46, doi:10.5194/amt-2-33-2009, 2009. 6082

Duncan, B. N.: Interannual and seasonal variability of biomass burning emissions constrained by satellite observations, *J. Geophys. Res.*, 108, 4100, doi:10.1029/2002JD002378, 2003. 6097

Ek, M. B., Mitchell, K. E., Lin, Y., Rogers, E., Grunmann, P., Koren, V., Gayno, G., and Tarp-ley, J. D.: Implementation of Noah land surface model advances in the National Centers for Environmental Prediction operational mesoscale Eta model, *J. Geophys. Res.*, 108, 8851, doi:10.1029/2002JD003296, 2003. 6120

Emmons, L. K., Walters, S., Hess, P. G., Lamarque, J.-F., Pfister, G. G., Fillmore, D., Granier, C., Guenther, A., Kinnison, D., Laepple, T., Orlando, J., Tie, X., Tyndall, G., Wiedinmyer, C., Baughcum, S. L., and Kloster, S.: Description and evaluation of the Model for Ozone and Related chemical Tracers, version 4 (MOZART-4), *Geosci. Model Dev.*, 3, 43–67, doi:10.5194/gmd-3-43-2010, 2010. 6079

Fast, J. D., Gustafson, W. I., Easter, R. C., Zaveri, R. A., Barnard, J. C., Chapman, E. G., Grell, G. A., and Peckham, S. E.: Evolution of ozone, particulates, and aerosol direct radiative forcing in the vicinity of Houston using a fully coupled meteorology-chemistry-aerosol model, *J. Geophys. Res.*, 111, 1–29, doi:10.1029/2005JD006721, 2006. 6070

Flemming, J., Peuch, V.-H., Engelen, R., and Kaiser, J.: A European global-to-regional that combines modeling: a novel forecasting system for atmospheric composition operates daily to forecast global air pollution, *EM: Air and Waste Management Association's Magazine for Environmental Managers*, 6–10, 2013. 6079

Freitas, S. R., Longo, K. M., Chatfield, R., Latham, D., Silva Dias, M. A. F., Andreae, M. O., Prins, E., Santos, J. C., Gielow, R., and Carvalho Jr., J. A.: Including the sub-grid scale plume rise of vegetation fires in low resolution atmospheric transport models, *Atmos. Chem.*

**SAMBBA WRF-Chem setup**

S. Archer-Nicholls et al.

[Title Page](#)[Abstract](#)[Introduction](#)[Conclusions](#)[References](#)[Tables](#)[Figures](#)[◀](#)[▶](#)[◀](#)[▶](#)[Back](#)[Close](#)[Full Screen / Esc](#)[Printer-friendly Version](#)[Interactive Discussion](#)

Freitas, S. R., Longo, K. M., Silva Dias, M. A. F., Chatfield, R., Silva Dias, P., Artaxo, P., Andreae, M. O., Grell, G., Rodrigues, L. F., Fazenda, A., and Panetta, J.: The Coupled Aerosol and Tracer Transport model to the Brazilian developments on the Regional Atmospheric Modeling System (CATT-BRAMS) – Part 1: Model description and evaluation, *Atmos. Chem. Phys.*, 9, 2843–2861, doi:10.5194/acp-9-2843-2009, 2009. 6065, 6066, 6075, 6079, 6098

Freitas, S. R., Longo, K. M., Trentmann, J., and Latham, D.: Technical Note: Sensitivity of 1-D smoke plume rise models to the inclusion of environmental wind drag, *Atmos. Chem. Phys.*, 10, 585–594, doi:10.5194/acp-10-585-2010, 2010. 6073, 6074

Freitas, S. R., Longo, K. M., Alonso, M. F., Pirre, M., Marecal, V., Grell, G., Stockler, R., Mello, R. F., and Sánchez Gáctica, M.: PREP-CHEM-SRC – 1.0: a preprocessor of trace gas and aerosol emission fields for regional and global atmospheric chemistry models, *Geosci. Model Dev.*, 4, 419–433, doi:10.5194/gmd-4-419-2011, 2011. 6064, 6067, 6078, 6079, 6084, 6085

Giglio, L.: Characterization of the tropical diurnal fire cycle using VIRS and MODIS observations, *Remote Sens. Environ.*, 108, 407–421, doi:10.1016/j.rse.2006.11.018, 2007. 6078

Giglio, L. and Kendall, J. D.: Application of the Dozier retrieval to wildfire characterization – a sensitivity analysis, *Remote Sens. Environ.*, 77, 34–49, 2001. 6075

Giglio, L. and Justice, C. O.: Effect of wavelength selection on characterization of fire size and temperature, *Int. J. Remote Sens.*, 24, 3515–3520, 2003. 6075

Giglio, L. and Schroeder, W.: A global feasibility assessment of the bi-spectral fire temperature and area retrieval using MODIS data, *Remote Sens. Environ.*, 152, 166–173, doi:10.1016/j.rse.2014.06.010, 2014. 6075

Giglio, L., Desclores, J., Justice, C. O., and Kaufman, Y. J.: An enhanced contextual fire detection algorithm for MODIS, *Remote Sens. Environ.*, 87, 273–282, doi:10.1016/S0034-4257(03)00184-6, 2003. 6071

Grell, G. and Baklanov, A.: Integrated modeling for forecasting weather and air quality: a call for fully coupled approaches, *Atmos. Environ.*, 45, 6845–6851, doi:10.1016/j.atmosenv.2011.01.017, 2011. 6064, 6068

Grell, G. A. and Devenyi, D.: A generalized approach to parameterizing convection combining ensemble and data assimilation techniques, *Geophys. Res. Lett.*, 29, 10–13, doi:10.1029/2002GL015311, 2002. 6120

SAMBBA WRF-Chem setup

S. Archer-Nicholls et al.

[Title Page](#)

[Abstract](#)

[Introduction](#)

[Conclusions](#)

[References](#)

[Tables](#)

[Figures](#)

◀

▶

◀

▶

[Back](#)

[Close](#)

[Full Screen / Esc](#)

[Printer-friendly Version](#)

[Interactive Discussion](#)



Grell, G. A., Peckham, S. E., Schmitz, R., McKeen, S. A., Frost, G., Skamarock, W. C., and Eder, B.: Fully coupled “online” chemistry within the WRF model, *Atmos. Environ.*, 39, 6957–6975, doi:10.1016/j.atmosenv.2005.04.027, 2005. 6066, 6068

Grell, G., Freitas, S. R., Stuefer, M., and Fast, J.: Inclusion of biomass burning in WRF-Chem: impact of wildfires on weather forecasts, *Atmos. Chem. Phys.*, 11, 5289–5303, doi:10.5194/acp-11-5289-2011, 2011. 6065, 6066

Guenther, A., Karl, T., Harley, P., Wiedinmyer, C., Palmer, P. I., and Geron, C.: Estimates of global terrestrial isoprene emissions using MEGAN (Model of Emissions of Gases and Aerosols from Nature), *Atmos. Chem. Phys.*, 6, 3181–3210, doi:10.5194/acp-6-3181-2006, 2006. 6085

Haywood, J. and Boucher, O.: Estimates of the direct and indirect radiative forcing due to tropospheric aerosols: a review, *Rev. Geophys.*, 38, 513, doi:10.1029/1999RG000078, 2000. 6064

Heim, M., Mullins, B. J., Umhauer, H., and Kasper, G.: Performance evaluation of three optical particle counters with an efficient multimodal calibration method, *J. Aerosol Sci.*, 39, 1019–1031, doi:10.1016/j.jaerosci.2008.07.006, 2008. 6083, 6121

Holben, B. N., Eck, T. F., Slutsker, I., Tanre, D., Buis, J. P., Setzer, A., Vermote, E., Reagan, J. A., Kaufman, Y. J., Nakajima, T., Lavenu, F., Jankowiak, I., and Smirnov, A.: AERONET – a federated instrument network and data archive for aerosol characterization, *Remote Sens. Environ.*, 66, 1–16, 1998. 6082

Holben, N., Tanré, D., Smirnov, A., Eck, T. F., Slutsker, I., Newcomb, W. W., Schafer, J. S., Chatenet, B., Lavenu, F., Kaufman, J., Vande Castle, J., Setzer, A., Markham, B., Clark, D., Halthore, R., Karneli, A., Neill, N. T. O., Pietras, C., Pinker, T., Voss, K., and Zibordi, G.: An emerging ground-based aerosol climatology: aerosol optical depth from AERONET, *J. Geophys. Res.*, 106, 12067–12097, 2001. 6068, 6082

Hollingsworth, A., Engelen, R. J., Benedetti, A., Dethof, A., Flemming, J., Kaiser, J. W., Morcrette, J.-J., Simmons, a. J., Textor, C., Boucher, O., Chevallier, F., Rayner, P., Elbern, H., Eskes, H., Granier, C., Peuch, V.-H., Rouil, L., and Schultz, M. G.: Toward a monitoring and forecasting system for atmospheric composition: the GEMS project, *B. Am. Meteorol. Soc.*, 89, 1147–1164, doi:10.1175/2008BAMS2355.1, 2008. 6079

Hong, S.-Y., Noh, Y., and Dudhia, J.: Ew vertical diffusion package with an explicit treatment of entrainment processes, *Mon. Weather Rev.*, 134, 2318–2341, doi:10.1175/MWR3199.1, 2006. 6120

## SAMBBA WRF-Chem setup

S. Archer-Nicholls et al.

[Title Page](#)[Abstract](#)[Introduction](#)[Conclusions](#)[References](#)[Tables](#)[Figures](#)[◀](#)[▶](#)[◀](#)[▶](#)[Back](#)[Close](#)[Full Screen / Esc](#)[Printer-friendly Version](#)[Interactive Discussion](#)

## SAMBBA WRF-Chem setup

S. Archer-Nicholls et al.

[Title Page](#)[Abstract](#)[Introduction](#)[Conclusions](#)[References](#)[Tables](#)[Figures](#)[◀](#)[▶](#)[◀](#)[▶](#)[Back](#)[Close](#)[Full Screen / Esc](#)[Printer-friendly Version](#)[Interactive Discussion](#)

Huneeus, N., Chevallier, F., and Boucher, O.: Estimating aerosol emissions by assimilating observed aerosol optical depth in a global aerosol model, *Atmos. Chem. Phys.*, 12, 4585–4606, doi:10.5194/acp-12-4585-2012, 2012. 6065

Huffman, G. J., Adler, R. F., Morrissey, M. M., Bolvin, D. T., Curtis, S., Joyce, R., McGavock, B., Susskind, J.: Global precipitation at one-degree daily resolution from multisatellite observations, *J. Hydrometeorol.*, 2, 36–50, doi:10.1175/1525-7541(2001)002<0036:GPAODD>2.0.CO;2, 2001. 6081, 6087, 6124

Huffman, G. J., Stocker, E. F., Bolvin, D. T., Nelkin, E. J., and Adler, R. F.: TRMM Version 7 3B42 and 3B43 Data Sets. NASA/GSFC, Greenbelt, MD, available at: <http://mirador.gsfc.nasa.gov/cgi-bin/mirador/presentNavigation.pl?project=TRMM&tree=project> (last access: 16 September 2014), last updated 2013. 6081, 6087, 6124

Ichoku, C. and Ellison, L.: Global top-down smoke-aerosol emissions estimation using satellite fire radiative power measurements, *Atmos. Chem. Phys.*, 14, 6643–6667, doi:10.5194/acp-14-6643-2014, 2014. 6065

Ichoku, C., Kahn, R., and Chin, M.: Satellite contributions to the quantitative characterization of biomass burning for climate modeling, *Atmos. Res.*, 111, 1–28, doi:10.1016/j.atmosres.2012.03.007, 2012. 6065, 6066, 6074, 6096

Ignotti, E., Valente, J. G., Longo, K. M., Freitas, S. R., Hacon, S. de S., and Artaxo, P.: Impact on human health of particulate matter emitted from burnings in the Brazilian Amazon region, *Rev. Saude Publ.*, 44, 121–130, 2010. 6064

Inness, A., Baier, F., Benedetti, A., Bouarar, I., Chabriat, S., Clark, H., Clerbaux, C., Coheur, P., Engelen, R. J., Errera, Q., Flemming, J., George, M., Granier, C., Hadji-Lazaro, J., Huijnen, V., Hurtmans, D., Jones, L., Kaiser, J. W., Kapsomenakis, J., Lefever, K., Leitão, J., Razinger, M., Richter, A., Schultz, M. G., Simmons, A. J., Suttie, M., Stein, O., Thépaut, J.-N., Thouret, V., Vrekoussis, M., Zerefos, C., and the MACC team: The MACC reanalysis: an 8 yr data set of atmospheric composition, *Atmos. Chem. Phys.*, 13, 4073–4109, doi:10.5194/acp-13-4073-2013, 2013. 6079

Janhäll, S., Andreae, M. O., and Pöschl, U.: Biomass burning aerosol emissions from vegetation fires: particle number and mass emission factors and size distributions, *Atmos. Chem. Phys.*, 10, 1427–1439, doi:10.5194/acp-10-1427-2010, 2010. 6077, 6078, 6118

Jimenez, J. L., Canagaratna, M. R., Donahue, N. M., Prevot, A. S. H., Zhang, Q., Kroll, J. H., DeCarlo, P. F., Allan, J. D., Coe, H., Ng, N. L., Aiken, A. C., Docherty, K. S., Ulbrich, I. M., Grieshop, A., P., Robinson, A. L., Duplissy, J., Smith, J. D., Wilson, K., R., Lanz, V. A.,

5 Hueglin, C., Sun, Y. L., Tian, J., Laaksonen, A., Raatikainen, T., Rautiainen, J., Vaattovaara, P., Ehn, M., Kulmala, M., Tomlinson, J. M., Collins, D. R., Cubison, M. J., Dunlea, E. J., Huffman, J. A., Onasch, T. B., Alfarra, M. R., Williams, P. I., Bower, K., Kondo, Y., Schneider, J., Drewnick, F., Borrmann, S., Weimer, S., Demerjian, K., Salcedo, D., Cottrell, L., Griffin, R., Takami, A., Miyoshi, T., Hatakeyama, S., Shimono, A., Sun, J. Y., Zhang, Y., M., Dzepina, K., Kimmel, J., R., Sueper, D., Jayne, J. T., Herndon, S. C., Trimborn, A. M., Williams, L. R., Wood, E. C., Middlebrook, A. M., Kolb, C. E., Baltensperger, U., Worsnop, D. R.: Evolution of organic aerosols in the atmosphere, *Science*, 326, 1525–1529, doi:10.1126/science.1180353, 2009. 6094

10 Jolley, M. D., Coe, H., McFiggans, G., Capes, G., Allan, J. D., Crosier, J., Williams, P. I., Allen, G., Bower, K. N., Jimenez, J. L., Russell, L. M., Grutter, M., and Baumgardner, D.: Characterizing the aging of biomass burning organic aerosol by use of mixing ratios: a meta-analysis of four regions, *Environ. Sci. Technol.*, 46, 13093–13102, doi:10.1021/es302386v, 2012. 6069, 6094

15 Kaiser, J. W., Flemming, J., Schultz, M. G., Suttie, M., and Wooster, M. J.: The Global Fire Assimilation System: First Emission Products (GFAv0), Tech. Memo. 596, ECMWF, Reading, UK, 2009. 6078, 6079

20 Kaiser, J. W., Heil, A., Andreae, M. O., Benedetti, A., Chubarova, N., Jones, L., Morcrette, J.-J., Razinger, M., Schultz, M. G., Suttie, M., and van der Werf, G. R.: Biomass burning emissions estimated with a global fire assimilation system based on observed fire radiative power, *Biogeosciences*, 9, 527–554, doi:10.5194/bg-9-527-2012, 2012. 6065, 6072, 6079, 6096

25 Kessler, E.: On the Distribution and Continuity of Water Substance in Atmospheric Circulation Models, *Meteorol. Monogr.*, Vol. 10, Am. Meteorol. Soc., Boston, MA, 1969. 6072

30 Kotchenruther, R. A. and Hobbs, P. V: Humidification factors of aerosols from biomass burning in Brazil, *J. Geophys. Res.*, 103, 32081, doi:10.1029/98JD00340, 1998. 6083

Lack, D. A., Langridge, J. M., Bahreini, R., Cappa, C. D., Middlebrook, A. M., and Schwarz, J. P.: Brown carbon and internal mixing in biomass burning particles, *P. Natl. Acad. Sci. USA*, 109, 14802–14807, doi:10.1073/pnas.1206575109, 2012. 6070, 6099

Lack, D. A., Bahreini, R., Langridge, J. M., Gilman, J. B., and Middlebrook, A. M.: Brown carbon absorption linked to organic mass tracers in biomass burning particles, *Atmos. Chem. Phys.*, 13, 2415–2422, doi:10.5194/acp-13-2415-2013, 2013. 6070, 6099

Longo, K. M., Freitas, S. R., Andreae, M. O., Setzer, A., Prins, E., and Artaxo, P.: The Coupled Aerosol and Tracer Transport model to the Brazilian developments on the Regional

[Title Page](#)[Abstract](#)[Introduction](#)[Conclusions](#)[References](#)[Tables](#)[Figures](#)[◀](#)[▶](#)[◀](#)[▶](#)[Back](#)[Close](#)[Full Screen / Esc](#)[Printer-friendly Version](#)[Interactive Discussion](#)

5 Martin, S. T., Andreae, M. O., Artaxo, P., Baumgardner, D., Chen, Q., Goldstein, A. H., Guenther, A., Heald, C. L., Bracero, O. L. M., McMurry, P. H., Pauliquevis, T., Pöschl, U., Prather, K. A., Roberts, G. C., Saleska, S. R., Silva-Dias, M. A., Spracklen, D. V., Swietlicki, E. T.: Sources and properties of amazonian aerosol particles, *Rev. Geophys.*, 48, 1–42, doi:10.1029/2008RG000280, 2010. 6086

10 Matsui, H., Koike, M., Kondo, Y., Moteki, N., Fast, J. D., and Zaveri, R. A.: Development and validation of a black carbon mixing state resolved three-dimensional model: Aging processes and radiative impact, *J. Geophys. Res. Atmos.*, 118, 2304–2326, doi:10.1029/2012JD018446, 2013. 6070, 6095, 6099

15 McFiggans, G., Artaxo, P., Baltensperger, U., Coe, H., Facchini, M. C., Feingold, G., Fuzzi, S., Gysel, M., Laaksonen, A., Lohmann, U., Mentel, T. F., Murphy, D. M., O'Dowd, C. D., Snider, J. R., and Weingartner, E.: The effect of physical and chemical aerosol properties on warm cloud droplet activation, *Atmos. Chem. Phys.*, 6, 2593–2649, doi:10.5194/acp-6-2593-2006, 2006. 6064

20 McMeeking, G. R., Hamburger, T., Liu, D., Flynn, M., Morgan, W. T., Northway, M., Highwood, E. J., Krejci, R., Allan, J. D., Minikin, A., and Coe, H.: Black carbon measurements in the boundary layer over western and northern Europe, *Atmos. Chem. Phys.*, 10, 9393–9414, doi:10.5194/acp-10-9393-2010, 2010. 6082

25 Middlebrook, A. M., Bahreini, R., Jimenez, J. L., and Canagaratna, M. R.: Evaluation of composition-dependent collection efficiencies for the aerodyne aerosol mass spectrometer using field data, *Aerosol Sci. Tech.*, 46, 258–271, doi:10.1080/02786826.2011.620041, 2012. 6082

30 Mlawer, E. J., Taubman, S. J., Brown, P. D., Iacono, M. J., and Clough, S. A.: Radiative transfer for inhomogeneous atmospheres: RRTM, a validated correlated-k model for the longwave, *J. Geophys. Res.*, 102, 16663–16682, doi:10.1029/97JD00237, 1997. 6084, 6120

Morgan, W. T., Allan, J. D., Bower, K. N., Capes, G., Crosier, J., Williams, P. I., and Coe, H.: Vertical distribution of sub-micron aerosol chemical composition from North-Western Europe and the North-East Atlantic, *Atmos. Chem. Phys.*, 9, 5389–5401, doi:10.5194/acp-9-5389-2009, 2009. 6082, 6121

SAMBBA WRF-Chem setup

S. Archer-Nicholls et al.

[Title Page](#)

[Abstract](#)

[Introduction](#)

[Conclusions](#)

[References](#)

[Tables](#)

[Figures](#)

◀

▶

◀

▶

[Back](#)

[Close](#)

[Full Screen / Esc](#)

[Printer-friendly Version](#)

[Interactive Discussion](#)



Morgan, W. T., Allan, J. D., Flynn, M., Darbyshire, E., Hodgson, A., Johnson, B. T., Haywood, J. M. Freitas, S., Longo, K., Artaxo, P., and Coe, H.: Overview of the South American biomass burning analysis (SAMBBA) field experiment, AIP Conf. Proc., 1527, 587–590, doi:10.1063/1.4803339, 2013. 6067

5 Morcrette, J.-J., Boucher, O., Jones, L., Salmond, D., Bechtold, P., Beljaars, A., Benedetti, A., Bonet, A., Kaiser, J. W., Razinger, M., Schulz, M., Serrar, S., Simmons, A. J., Sofiev, M., Suttie, M., Tompkins, A. M., and Untch, A.: Aerosol analysis and forecast in the European Centre for Medium-Range Weather Forecasts Integrated Forecast System: forward modeling, *J. Geophys. Res.*, 114, D06206, doi:10.1029/2008JD011235, 2009. 6080, 6119

10 Morrison, H., Curry, J. A., and Khvorostyanov, V. I.: A new double-moment microphysics parameterization for application in cloud and climate models. Part I: Description, *J. Atmos. Sci.*, 62, 1665–1677, doi:10.1175/JAS3446.1, 2005. 6120

Müller, T., Laborde, M., Kassell, G., and Wiedensohler, A.: Design and performance of a three-wavelength LED-based total scatter and backscatter integrating nephelometer, *Atmos. Meas. Tech.*, 4, 1291–1303, doi:10.5194/amt-4-1291-2011, 2011. 6082

15 Pereira, G., Freitas, S. R., Moraes, E. C., Ferreira, N. J., Shimabukuro, Y. E., Rao, V. B., and Longo, K. M.: Estimating trace gas and aerosol emissions over South America: relationship between fire radiative energy released and aerosol optical depth observations, *Atmos. Environ.*, 43, 6388–6397, doi:10.1016/j.atmosenv.2009.09.013, 2009. 6065

20 Peterson, D. and Wang, J.: A sub-pixel-based calculation of the fire radiative power from MODIS observations: 2. Sensitivity analysis and potential fire weather application, *Remote Sens. Environ.*, 129, 231–249, doi:10.1016/j.rse.2012.10.020, 2013. 6075

Peterson, D., Wang, J., Ichoku, C., Hyer, E., and Ambrosia, V.: A sub-pixel-based calculation of the fire radiative power from MODIS observations: 1. Algorithm development and initial assessment, *Remote Sens. Environ.*, 129, 262–279, doi:10.1016/j.rse.2012.10.036, 2013. 6075

25 Petrenko, M., Kahn, R., Chin, M., Soja, A., and Kucsera, T.: The use of satellite-measured aerosol optical depth to constrain biomass burning emissions source strength in the global model GOCART, *J. Geophys. Res. Atmos.*, 117, D18212, doi:10.1029/2012JD017870, 2012. 6072

30 Pincus, R., Barker, H. W., and Morcrette, J.-J.: A fast, flexible, approximate technique for computing radiative transfer in inhomogeneous cloud fields, *J. Geophys. Res.*, 108, 4376, doi:10.1029/2002JD003322, 2003. 6084, 6120

[Title Page](#)[Abstract](#)[Introduction](#)[Conclusions](#)[References](#)[Tables](#)[Figures](#)[◀](#)[▶](#)[◀](#)[▶](#)[Back](#)[Close](#)[Full Screen / Esc](#)[Printer-friendly Version](#)[Interactive Discussion](#)

Prins, E. M., Feltz, J. M., Menzel, W. P., and Ward, D. E.: An overview of GOES-8 diurnal fire and smoke results for SCAR-B and 1995 fire season in South America, *J. Geophys. Res.*, 103, 31821–31835, 1998. 6071

Ogren, J. A.: Comment on “Calibration and intercomparison of filter-based measurements of visible light absorption by aerosols”, *Aerosol Sci. Tech.*, 44, 589–591, doi:10.1080/02786826.2010.482111, 2010. 6083, 6121

Ogura, Y. and Takahashi, T.: Numerical simulation of the life cycle of a thunderstorm cell, *Mon. Weather Rev.*, 99, 895–911, 1971. 6072

Olivier, J. G. J., Berdowski, J. J. M., Jeroen, A. H. W., Bakker, J., Visschedijk, A. J. H., and Bloos, J. J.: Applications of EDGAR Including a Description of EDGAR 3.2: Reference Database with Trend Data for 1970–1995, RIVM report no. 773301 001/NOP report no. 410200 051, RIVM, Bilthoven, 2002. 6085

Olson, J. S., Watts, J. A., and Allison, L. J.: Major World Ecosystem Complexes Ranked by Carbon in Live Vegetation: A Database (Revised November 2000), NDP-017, available online at: <http://cdiac.esd.ornl.gov/ndps/ndp017.html> (last access: 16 September 2014), Carbon Dioxide Information Analysis Center, Oak Ridge National Laboratory, Oak Ridge, Tennessee, USA, 2000. 6071

Randerson, J. T., Chen, Y., van der Werf, G. R., Rogers, B. M., and Morton, D. C.: Global burned area and biomass burning emissions from small fires, *J. Geophys. Res.*, 117, G04012, doi:10.1029/2012JG002128, 2012. 6097

Rizzo, L. V., Artaxo, P., Müller, T., Wiedensohler, A., Paixão, M., Cirino, G. G., Arana, A., Swietlicki, E., Roldin, P., Fors, E. O., Wiedemann, K. T., Leal, L. S. M., and Kulmala, M.: Long term measurements of aerosol optical properties at a primary forest site in Amazonia, *Atmos. Chem. Phys.*, 13, 2391–2413, doi:10.5194/acp-13-2391-2013, 2013. 6079

Reid, S. and Hobbs, P. V.: Physical and optical properties of young smoke from individual biomass fires in Brazil, *J. Geophys. Res.*, 103, 32013–32030, 1998. 6077, 6078

Reid, J. S., Koppmann, R., Eck, T. F., and Eleuterio, D. P.: A review of biomass burning emissions part II: intensive physical properties of biomass burning particles, *Atmos. Chem. Phys.*, 5, 799–825, doi:10.5194/acp-5-799-2005, 2005. 6077

Remer, L. A., Kaufman, Y. J., Tanr, D., Mattoo, S., Chu, D. a., Martins, J. V., Li, R.-R., Ichoku, C., Levy, R. C., Kleidman, R. G., Eck, T. F., Vermote, E., and Holben, B. N.: The MODIS aerosol algorithm, products, and validation, *J. Atmos. Sci.*, 62, 947–973, doi:10.1175/JAS3385.1, 2005. 6081

Roberts, G. C. and Nenes, A.: A continuous-flow streamwise thermal-gradient CCN chamber for atmospheric measurements, *Aerosol Sci. Tech.*, 39, 206–221, doi:10.1080/027868290913988, 2005. 6083, 6121

5 Saleh, R., Robinson, E. S., Tkacik, D. S., Ahern, A. T., Liu, S., Aiken, A. C., Sullivan, R. C., Presto, A. A., Dubey, M. K., Yokelson, R. J., Donahue, N. M., and Robinson, A. L.: Brownness of organics in aerosols from biomass burning linked to their black carbon content, *Nat. Geosci.*, 7, 647–650, doi:10.1038/ngeo2220, 2014. 6070, 6099

10 Samset, B. H. and Myhre, G.: Vertical dependence of black carbon, sulphate and biomass burning aerosol radiative forcing, *Geophys. Res. Lett.*, 38, L24802, doi:10.1029/2011GL049697, 2011. 6067

15 Samset, B. H., Myhre, G., Schulz, M., Balkanski, Y., Bauer, S., Berntsen, T. K., Bian, H., Bel-  
louin, N., Diehl, T., Easter, R. C., Ghan, S. J., Iversen, T., Kinne, S., Kirkevåg, A., Lamar-  
que, J.-F., Lin, G., Liu, X., Penner, J. E., Seland, Ø., Skeie, R. B., Stier, P., Takemura, T.,  
Tsigaridis, K., and Zhang, K.: Black carbon vertical profiles strongly affect its radiative forc-  
ing uncertainty, *Atmos. Chem. Phys.*, 13, 2423–2434, doi:10.5194/acp-13-2423-2013, 2013.  
6067

20 Schwarz, J. P., Gao, R. S., Spackman, J. R., Watts, L. A., Thomson, D. S., Fahey, D. W., Ry-  
erson, T. B., Peischl, J., Holloway, J. S., Trainer, M., Frost, G. J., Baynard, T., Lack, D. A.,  
de Gouw, J. A., Warneke, C., and Del Negro, L. A.: Measurement of the mixing state, mass,  
and optical size of individual black carbon particles in urban and biomass burning emissions,  
25 *Geophys. Res. Lett.*, 35, L13810, doi:10.1029/2008GL033968, 2008. 6082

25 Sestini, M., Reimer, E., Valeriano, D., Alvalá, R., Mello, E., Chan, C., and Nobre, C.: Mapa de  
cobertura da terra da Amazônia legal para uso em modelos meteorológicos, in: *Anais XI  
Simpósio Brasileiro de Sensoriamento Remoto*, 2901–2906, 2003. 6071, 6084

30 Setzer, A. and Pereira, M.: Amazonia biomass burnings in 1987 and an estimate of their tropo-  
spheric emissions, *Ambio*, 20, 19–22, 1991. 6071

35 Shimabukuro, Y. E., Pereira, G., Cardozo, F. S., Stockler, R., Freitas, S. R., and Coura, S. M. C.:  
Biomass burning emission estimation in Amazon tropical forest, in: *Earth Observation of  
Ecosystem Services*, 1st Edn., edited by: Segura, D. A., Di Bella, C. M., Straschnoy, J. V.,  
Taylor & Francis, Oxford, UK, 112–130, 2013. 6075, 6076

40 Shiraiwa, M., Kondo, Y., Moteki, N., Takegawa, N., Sahu, L. K., Takami, A., Hatakeyama, S.,  
Yonemura, S., and Blake, D. R.: Radiative impact of mixing state of black carbon aerosol in  
Asian outflow, *J. Geophys. Res.*, 113, D24210, doi:10.1029/2008JD010546, 2008. 6082

## SAMBBA WRF-Chem setup

[Title Page](#)[Abstract](#)[Introduction](#)[Conclusions](#)[References](#)[Tables](#)[Figures](#)[◀](#)[▶](#)[◀](#)[▶](#)[Back](#)[Close](#)[Full Screen / Esc](#)[Printer-friendly Version](#)[Interactive Discussion](#)

Shrivastava, M., Fast, J., Easter, R., Gustafson Jr., W. I., Zaveri, R. A., Jimenez, J. L., Saide, P., and Hodzic, A.: Modeling organic aerosols in a megacity: comparison of simple and complex representations of the volatility basis set approach, *Atmos. Chem. Phys.*, 11, 6639–6662, doi:10.5194/acp-11-6639-2011, 2011. 6069, 6099

5 Shrivastava, M., Berg, L. K., Fast, J. D., Easter, R. C., Laskin, A., Chapman, E. G., Jr., Gustafson, W. I., Ying, L., Berkowitz, C. M.: Modeling aerosols and their interactions with shallow cumuli during the 2007 CHAPS field study, *J. Geophys. Res.-Atmos.*, 118, 1343–1360, doi:10.1029/2012JD018218, 2013. 6069, 6099

10 Stein, O., Flemming, J., Inness, A., and Kaiser, J. W.: Global reactive gases forecasts and reanalysis in the MACC project, *Journal of Integrative Environmental Sciences*, 9, 1–14, doi:10.1080/1943815X.2012.696545, 2012. 6079

15 Stephens, M., Turner, N., and Sandberg, J.: Particle identification by laser-induced incandescence in a solid-state laser cavity, *Appl. Optics*, 42, 3726–3736, 2003. 6082, 6121

20 Stockwell, W. R., Middleton, P., Chang, J. S., and Tang, X.: The second-generation regional acid deposition model chemical mechanism for regional air quality modeling, *J. Geophys. Res.*, 95, 16343–16367, 1990. 6066

25 Stockwell, W. R., Kirchner, F., Kuhn, M., and Seefeld, S.: A new mechanism for regional atmospheric chemistry modeling, *J. Geophys. Res.*, 102, 25847–25979, 1997. 6066

30 Streets, D. G., Bond, T. C., Lee, T., and Jang, C.: On the future of carbonaceous aerosol emissions, *J. Geophys. Res.*, 109, D24212, doi:10.1029/2004JD004902, 2004. 6064

Taylor, J. W., Allan, J. D., Allen, G., Coe, H., Williams, P. I., Flynn, M. J., Le Breton, M., Muller, J. B. A., Percival, C. J., Oram, D., Forster, G., Lee, J. D., Rickard, A. R., and Palmer, P. I.: Size-dependent wet removal of black carbon in Canadian biomass burning plumes, *Atmos. Chem. Phys. Discuss.*, 14, 19469–19513, doi:10.5194/acpd-14-19469-2014, 2014. 6067, 6095

Toon, O. B. and Ackerman, T. P.: Algorithms for the calculation of scattering by stratified spheres, *Appl. Optics*, 20, 3657–3660, 1981. 6070

Tosca, M. G., Randerson, J. T., and Zender, C. S.: Global impact of smoke aerosols from landscape fires on climate and the Hadley circulation, *Atmos. Chem. Phys.*, 13, 5227–5241, doi:10.5194/acp-13-5227-2013, 2013. 6072, 6096

Trembath, J. A.: Airborne CCN Measurements, Ph.D. thesis, School of Earth, Atmospheric and Environmental Sciences, University of Manchester, UK, 268 pp., available at: <https://www.escholar.manchester.ac.uk/item/?pid=uk-ac-man-scw:212956>, 2013. 6083, 6121

## SAMBBA WRF-Chem setup

S. Archer-Nicholls et al.

[Title Page](#)[Abstract](#)[Introduction](#)[Conclusions](#)[References](#)[Tables](#)[Figures](#)[◀](#)[▶](#)[◀](#)[▶](#)[Back](#)[Close](#)[Full Screen / Esc](#)[Printer-friendly Version](#)[Interactive Discussion](#)

Turnbull, K.: PSAP Corrections: Amendment to MRF Technical Note No. 31, OBR Technical Note, No. 80, Met Office, August 2010. 6083, 6121

Turpin, B. J. and Lim, H.-J.: Species contributions to  $PM_{2.5}$  mass concentrations: revisiting common assumptions for estimating organic mass, *Aerosol Sci. Tech.*, 35, 602–610, 2001. 6078, 6085

Vakkari, V., Kerminen, V.-M., Beukes, J. P., Tiitta, P., van Zyl, P. G., Josipovic, M., Venter, A. D., Jaars, K., Worsnop, D. R., Kulmala, M., and Laakso, L.: Rapid changes in biomass burning aerosols by atmospheric oxidation, *Geophys. Res. Lett.*, 41, 2644–2651, doi:10.1002/2014GL059396, 2014. 6069, 6078, 6094

Val Martin, M., Logan, J. A., Kahn, R. A., Leung, F.-Y., Nelson, D. L., and Diner, D. J.: Smoke injection heights from fires in North America: analysis of 5 years of satellite observations, *Atmos. Chem. Phys.*, 10, 1491–1510, doi:10.5194/acp-10-1491-2010, 2010. 6066, 6067, 6097

van der Werf, G. R., Randerson, J. T., Giglio, L., Collatz, G. J., Kasibhatla, P. S., and Arel-Iano Jr., A. F.: Interannual variability in global biomass burning emissions from 1997 to 2004, *Atmos. Chem. Phys.*, 6, 3423–3441, doi:10.5194/acp-6-3423-2006, 2006. 6065

van der Werf, G. R., Randerson, J. T., Giglio, L., Collatz, G. J., Mu, M., Kasibhatla, P. S., Morton, D. C., DeFries, R. S., Jin, Y., and van Leeuwen, T. T.: Global fire emissions and the contribution of deforestation, savanna, forest, agricultural, and peat fires (1997–2009), *Atmos. Chem. Phys.*, 10, 11707–11735, doi:10.5194/acp-10-11707-2010, 2010. 6065

Viegas, D. X.: Forest fire propagation, *Philos. T. Roy. Soc. A*, 356, 2907–2928, doi:10.1098/rsta.1998.0303, 1998. 6075

Wang, S. C. and Flagan, R. C.: Scanning electrical mobility spectrometer, *Aerosol Sci. Tech.*, 13, 230–240, doi:10.1080/02786829008959441, 1990. 6083, 6121

Wu, L., Su, H., and Jiang, J. H.: Regional simulations of deep convection and biomass burning over South America: 1. Model evaluations using multiple satellite data sets, *J. Geophys. Res.*, 116, D17208, doi:10.1029/2011JD016106 2011a. 6066, 6072, 6096

Wu, L., Su, H., and Jiang, J. H.: Regional simulations of deep convection and biomass burning over South America: 2. Biomass burning aerosol effects on clouds and precipitation, *J. Geophys. Res.*, 116, D17209, doi:10.1029/2011JD016106 2011b. 6066

Yevich, R. and Logan, J. A.: An assessment of biofuel use and burning of agricultural waste in the developing world, *Global Biogeochem. Cy.*, 17, 1095, doi:10.1029/2002GB001952, 2003. 6085, 6097

**SAMBBA WRF-Chem setup**

S. Archer-Nicholls et al.

[Title Page](#)[Abstract](#)[Introduction](#)[Conclusions](#)[References](#)[Tables](#)[Figures](#)[◀](#)[▶](#)[◀](#)[▶](#)[Back](#)[Close](#)[Full Screen / Esc](#)[Printer-friendly Version](#)[Interactive Discussion](#)

Zaveri, R. A. and Peters, L. K.: A new lumped structure photochemical mechanism for large-scale applications, *J. Geophys. Res.*, 104, 30387–30415, 1999. 6068, 6077, 6084

Zaveri, R. A., Easter, R. C., Fast, J. D., and Peters, L. K.: Model for Simulating Aerosol Interactions and Chemistry (MOSAIC), *J. Geophys. Res.*, 113, D132024, doi:10.1029/2007JD008782, 2008. 6067, 6068, 6069, 6084

5 Zhang, D. and Anthes, R. A.: High-resolution model of the planetary boundary layer – sensitivity tests and comparisons with SESAME-79 data, *J. Appl. Meteorol.*, 21, 1594–1609, 1982. 6120

10 Zhang, Y., Fu, R., Yu, H., Qian, Y., Dickinson, R., Silva Dias, M. A. F., da Silva Dias, P. L., and Fernandes, K.: Impact of biomass burning aerosol on the monsoon circulation transition over Amazonia, *Geophys. Res. Lett.*, 36, L10814, doi:10.1029/2009GL037180, 2009. 6064

GMDD

7, 6061–6131, 2014

---

## SAMBBA WRF-Chem setup

S. Archer-Nicholls et al.

---

[Title Page](#)

[Abstract](#)

[Introduction](#)

[Conclusions](#)

[References](#)

[Tables](#)

[Figures](#)

◀

▶

◀

▶

[Back](#)

[Close](#)

[Full Screen / Esc](#)

[Printer-friendly Version](#)

[Interactive Discussion](#)



**Table 1.** Table of fire area and size, derived from MODIS FRP measurements for the 2012 Brazilian fire season, prepared by G. Periera.

Biome	number of data points	Burned area [ha]	Active fire size [ha]	Ratio (S/A)
Forest	191 386	$4.3 \pm 8.3$	$1.15 \pm 2.30$	0.267
Mixed Forest	1756	$10.63 \pm 12.16$	$2.45 \pm 3.01$	0.305
Scrublands	95 681	$9.13 \pm 12.0$	$2.15 \pm 2.30$	0.235
Savanna/cerrado	226 493	$7.80 \pm 9.30$	$1.90 \pm 3.20$	0.244
Cropland	36 667	$9.72 \pm 10.4$	$1.33 \pm 2.46$	0.137

**Table 2.** Fractional apportionment of particulate emissions across the 8 MOSAIC size bins, showing range of particle diameters for each bin, primary anthropogenic emission size fraction and biomass burning emission fractions based on Janhäll et al. (2010).

Bin 1	Bin 2	Bin 3	Bin 4	Bin 5	Bin 6	Bin 7	Bin 8
Particle dry diameter (nm).							
39.1–78.1	78.1–156	156–313	313–625	625–1250	1250–2500	2500–5000	5000–10 000
Primary anthropogenic aerosol emission size fractions (fine mode, < 2.5 µm).							
0.06	0.045	0.245	0.40	0.10	0.15	0.0	0.0
Biomass burning aerosol emission size fractions, based on Janhäll et al. (2010).							
0.0092	0.1385	0.4548	0.3388	0.0567	0.0020	0.0	0.0

[Title Page](#)[Abstract](#)[Introduction](#)[Conclusions](#)[References](#)[Tables](#)[Figures](#)[◀](#)[▶](#)[◀](#)[▶](#)[Back](#)[Close](#)[Full Screen / Esc](#)[Printer-friendly Version](#)[Interactive Discussion](#)

## SAMBBA WRF-Chem setup

S. Archer-Nicholls et al.

**Table 3.** Fractional apportionment of aerosol loadings from MACC-II model to 8 MOSAIC size bins for initial and boundary conditions (Morcrette et al., 2009). Apportioning for MACC-II aerosol species black carbon (BC), organic aerosol (OA), sulphate aerosol (SULF), dust (DU) and sea salt (SS). Uses same MOSAIC dry particle diameters as Table 2.

Bin 1	Bin 2	Bin 3	Bin 4	Bin 5	Bin 6	Bin 7	Bin 8
BC, POM (hydrophobic and hygroscopic) and SULF.							
0.0246	0.1475	0.3506	0.3321	0.1253	0.0187	$1.1 \times 10^{-3}$	$2.4 \times 10^{-5}$
SS Bin 1: 0.03–0.5 µm.							
$1.1 \times 10^{-3}$	0.0312	0.3169	0.6502	0.0	0.0	0.0	0.0
SS Bin 2: 0.5–5.0 µm.							
0.0	0.0	0.0	0.01	0.04	0.164	0.786	0.0
SS Bin 3: 5.0–20 µm.							
0.0	0.0	0.0	0.0	0.0	0.0	0.0	0.5515
DU Bin 1: 0.03–0.5 µm.							
$2.1 \times 10^{-5}$	0.0023	0.0928	0.9049	0.0	0.0	0.0	0.0
DU Bin 2: 0.55–0.9 µm.							
0.0	0.0	0.0	0.1493	0.8507	0.0	0.0	0.0
DU Bin 3: 0.9–20 µm.							
0.0	0.0	0.0	0.0	0.0989	0.3736	0.3643	0.1415

**Table 4.** Summary of physical parameterisations used in WRF-Chem model runs.

Process	WRF-Chem Option	Reference
Microphysics	Morrison 2-moment	Morrison et al. (2005)
Aerosol Activation	Abdul-Razzak and Ghan	Abdul-Razzak and Ghan (2002)
Cumulus parameterisation	Grell 3-D	Grell and Devenyi (2002)
Planetary Boundary Layer	Yonsai University (YSU)	Hong et al. (2006)
Surface Layer	MM5 surface-layer similarity	Zhang and Anthes (1982)
Land-Surface Model	Unified NOAH land-surface	Ek et al. (2003)
Longwave Radiation	RRTMG	Mlawer et al. (1997)
Shortwave Radiation	RRTMG	Pincus et al. (2003)

Title Page

Abstract      Introduction

Conclusions      References

Tables      Figures

◀      ▶

◀      ▶

Back      Close

Full Screen / Esc

Printer-friendly Version

Interactive Discussion



# SAMBBA WRF-Chem setup

S. Archer-Nicholls et al.

**Table 5.** Table of instruments and flights used for model evaluation. Each flight shown to have Full-, Partial- or Insufficient-coverage for each instrument, where Full is > 80% coverage, partial is between 80% and 30%, and Insufficient is < 30%. Acronyms used for instruments: Single Particle Soot Photometer (SP2, Baumgardner et al., 2004; Stephens et al., 2003), compact Time of Flight Aerosol Mass Spectrometer (cToF-AMS, Drewnick et al., 2005; Canagaratna et al., 2007; Morgan et al., 2009), Aero-Laser AL5002 VUV resonance fluorescence gas analyser, 3-wavelength integrating nephelometer (Anderson et al., 1996), Particle Soot Absorption Photometer (PSAP) (Bond et al., 1999; Ogren et al., 2010; Turnbull, 2010), Scanning Mobility Particle Sizer (SMPS, Wang et al., 1990), a GRIMM model 1.108 Optical Particle Counter (OPC, Heim et al., 2008) and a DMT dual column Cloud Condensation Nuclei counter (CCNc) (Roberts and Nenes, 2005; Trembath, 2013). Mass and number mixing ratios given per unit volume at standard temperature and pressure ( $\text{sm}^{-3}$  or  $\text{scm}^{-3}$ ).

Instrument	Measurement	Units	B731	B734	B739	B742
SP2	BC	$\mu\text{g sm}^{-3}$	Insufficient	Full	Full	Full
cToF-AMS	POM	$\mu\text{g sm}^{-3}$	Partial	Full	Full	Full
AL5002 VUV	CO	ppbv	Full	Full	Full	Full
Dry Nephelometer	$b_{\text{scat}}$	$\text{km}^{-1}$	Partial	Full	Full	Full
PSAP	$b_{\text{abs}}$	$\text{km}^{-1}$	Partial	Full	Partial	Partial
SMPS	Number distribution (20–350 nm)	$\text{scm}^{-3}$	Partial	Full	Insufficient	Full
GRIMM	Number distribution (0.3–20 $\mu\text{m}$ )	$\text{scm}^{-3}$	Full	Full	Full	Full
CCNc	CCN Concentration	$\text{scm}^{-3}$	Full	Full	Insufficient	Full

## Title Page

## Abstract

## Introduction

## Conclusions

## References

## Tables

## Figures

1

▶

Back

Close

Full Screen / Esc

[Printer-friendly Version](#)

## Interactive Discussion



**SAMBBA WRF-Chem setup**

S. Archer-Nicholls et al.

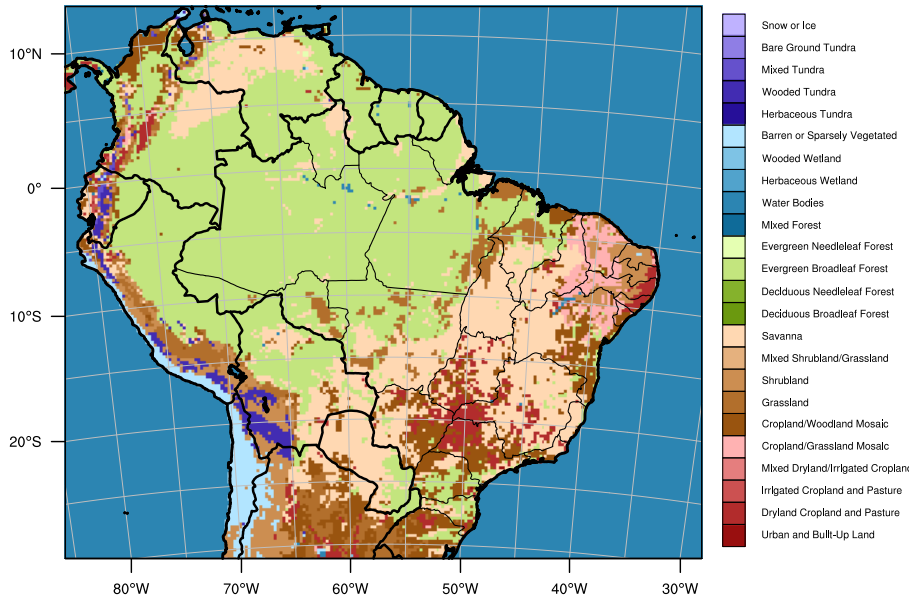


**Figure 1.** Map of domain used for study, at 25 km horizontal grid spacing with Lambert projection. Coloured by 24 USGS land-use categories. The southern Amazon, coloured green, is the main region of deforestation burning, corresponding to the West-central Brazilian states and northern Bolivia. The East-central Brazilian states, coloured pale-brown, are the main regions of cerrado burning.

## SAMBBA WRF-Chem setup

S. Archer-Nicholls et al.

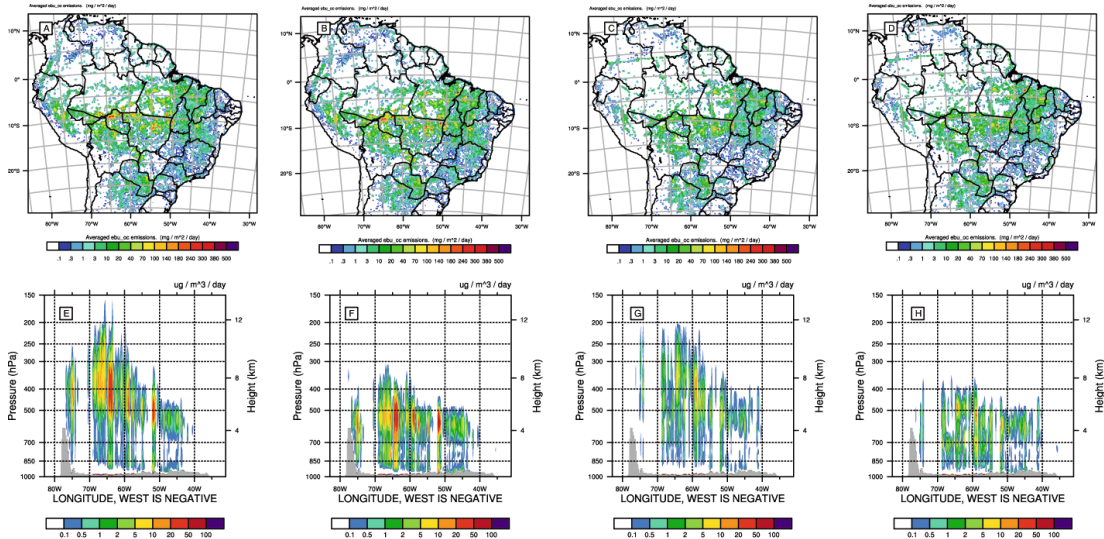


**Figure 2.** Emissions of organic aerosol (OA) over the course of the campaign. Panels (a–d) are maps of emissions, showing total emissions in the atmospheric column ( $\mu\text{g m}^{-2} \text{ day}^{-1}$ ). Panels (e–h) are vertical profiles of emissions through a transect along  $9^\circ \text{S}$  ( $\mu\text{g m}^{-2} \text{ day}^{-1}$ ). Panels (a), (b), (e) and (f) show averaged emissions over Phase I of the campaign (6–22 September 2012). (c), (d), (g) and (h) are averaged over Phase II (23–30 September). Panels (a), (c), (e) and (g) are for the traditional 3BEM emissions. Panels (b), (d), (f) and (h) are for the modified emissions, using smaller fire size and burned area depending on vegetation type as described in Table 1.



Title Page

Abstract

Introduction

Conclusions

References

Tables

Figures



Back

Close

Full Screen / Esc

Printer-friendly Version

Interactive Discussion

**SAMBBA WRF-Chem setup**

S. Archer-Nicholls et al.

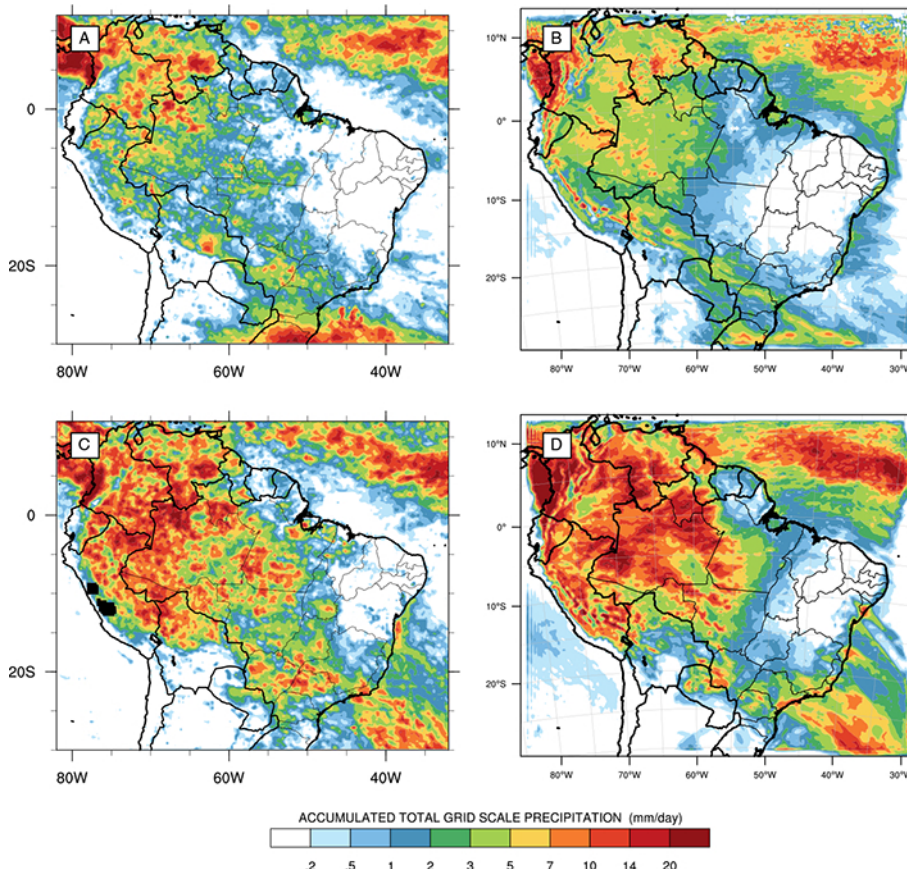


**Figure 3.** Maps of averaged precipitation ( $\text{mm day}^{-1}$ ). **(a and c)** are derived from the TRMM 3B42 satellite product (Huffman et al., 2001, 2013). **(b and d)** from WRF-Chem model runs. **(a and b)** for Phase I (6–22 September 2012), **(c and d)** over Phase II (23–30 September).

[Printer-friendly Version](#)[Interactive Discussion](#)[Title Page](#)[Abstract](#)[Introduction](#)[Conclusions](#)[References](#)[Tables](#)[Figures](#)[◀](#)[▶](#)[◀](#)[▶](#)[Back](#)[Close](#)[Full Screen / Esc](#)

## SAMBBA WRF-Chem setup

S. Archer-Nicholls et al.

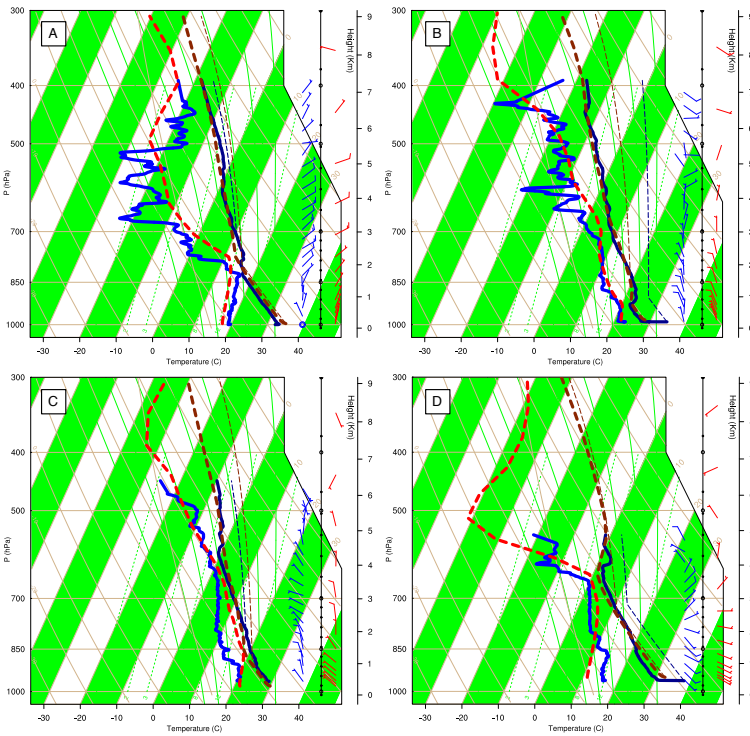


**Figure 4.** Skew-T plots comparing data from sondes dropped during SAMBBA flights with column data extracted from the WRF-Chem model at the time and place of the drop-sonde. Drop-sondes taken from **(a)** B731 (14 September, dropped at 16:02:28 UTC), **(b)** 734 (18 September, 12:46:52 UTC), **(c)** B737 (20 September, 15:23:59 UTC) and **(d)** B742 (27 September, 13:36:59 UTC). Red dashed lines from WRF-Chem model data, blue solid lines from drop-sonde. Eight coloured lines on left show dewpoint ( $^{\circ}\text{C}$ ), dark coloured lines on right show temperature ( $^{\circ}\text{C}$ ). Barbs on right of plots show wind direction from drop-sonde (blue) and model (red).

Full Screen / Esc

Printer-friendly Version

Interactive Discussion

## SAMBBA WRF-Chem setup

S. Archer-Nicholls et al.

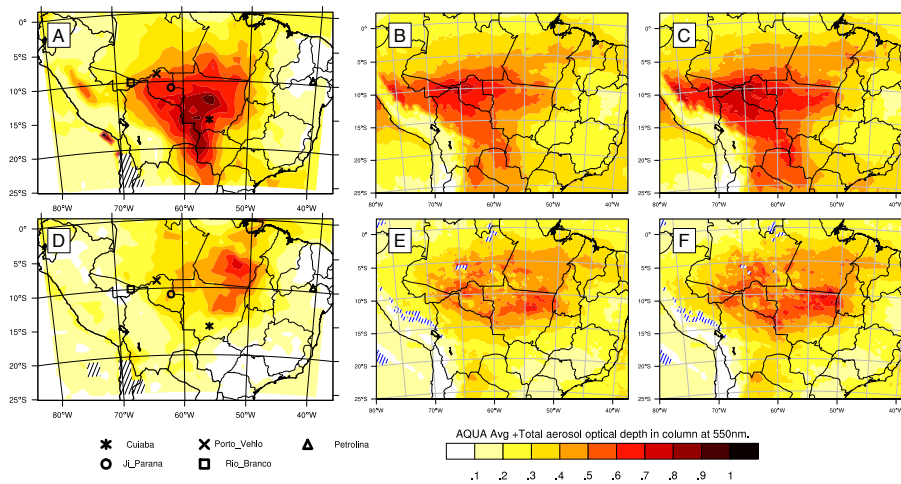


**Figure 5.** Horizontal map of column AOD at 550 nm, comparing the WRF-Chem model runs against MODIS Aqua and Terra satellites. **(a, b and c)** for the first phase of the campaign (6–22 September 2012), **(d, e and f)** averaged over the second phase of the campaign (23–30 September). **(a and d)** combined MODIS and TERRA satellite data. **(b and e)** from model runs using standard 3BEM emissions. **(c and f)** using, modified 3BEM emissions. The location of symbols in panels **(a and d)** signify the sites of the five operational AERONET sites during the campaign period.

[Title Page](#)[Abstract](#)[Introduction](#)[Conclusions](#)[References](#)[Tables](#)[Figures](#)[◀](#)[▶](#)[◀](#)[▶](#)[Back](#)[Close](#)[Full Screen / Esc](#)[Printer-friendly Version](#)[Interactive Discussion](#)

## SAMBBA WRF-Chem setup

S. Archer-Nicholls et al.

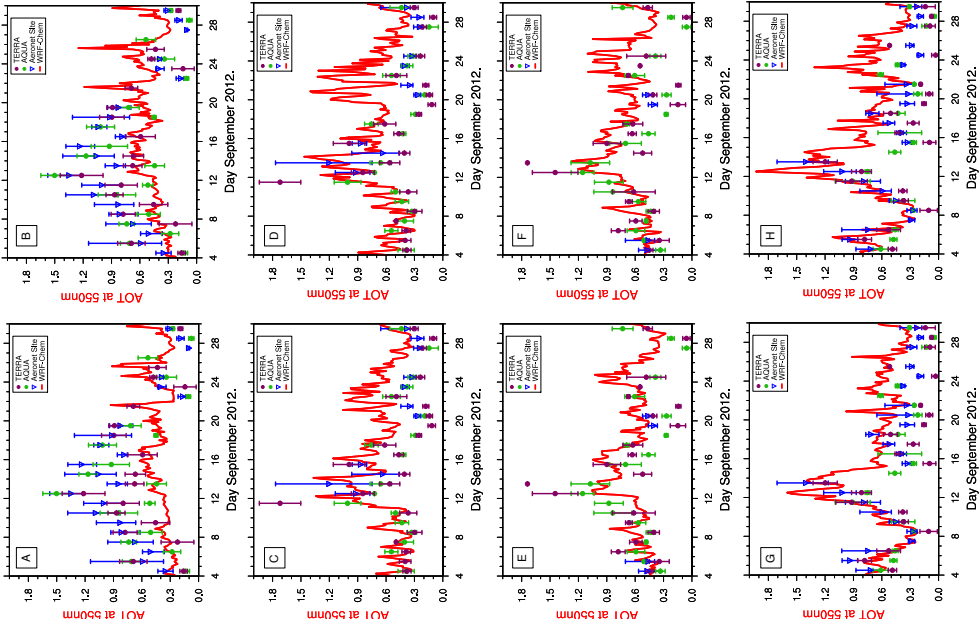


**Figure 6.** Timeseries of aerosol optical depth at 550 nm at four Aeronet sites between 4 September and 1 October 2012. **(a and b)** at Cuiaba, **(c and d)** at Porto Vehlo, **(e and f)** at Ji Parana and **(g and h)** at Rio Branco. Blue triangles show Aeronet Site daily measurements, with bars indicating range in values over the day. Purple and green circles indicate measurements from overpasses of TERRA and AQUA satellites respectively, with bars indicating error range. Red line shows data from WRF-Chem model, **(a, c, d and f)** from model run with traditional 3BEM emissions, **(b, d, f and h)** using modified emissions.

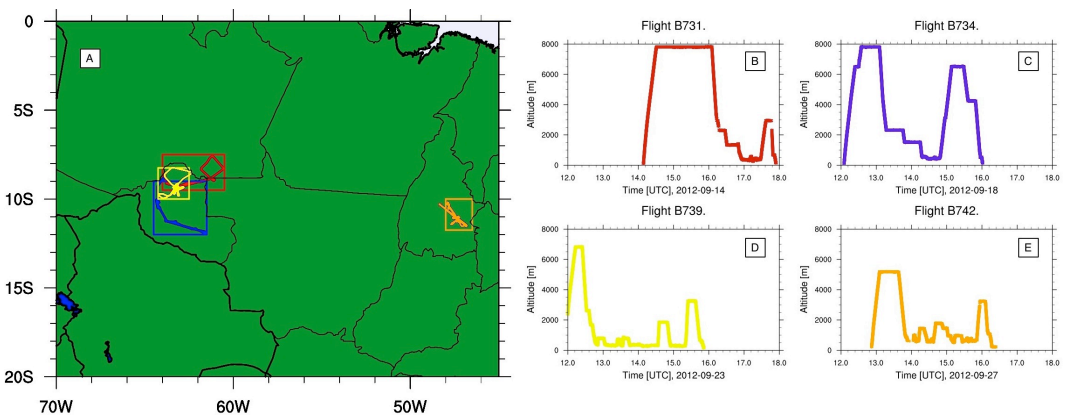


**Figure 7. (a)** Map of SAMBBA flight trajectories. Red: B731, 14 September 2012. Blue: B734, 18 September 2012. Yellow: B739, 23 September 2012. Orange: B742, 27 September 2012. Lines show path taken by flights, boxes show regions in model averaged over when comparing between model and flight data. **(b–e)**, altitude tracks of the four flights used for case-studies.

Title Page

Abstract      Introduction

Conclusions      References

Tables      Figures

◀      ▶

◀      ▶

Back      Close

Full Screen / Esc

Printer-friendly Version

Interactive Discussion



## SAMBBA WRF-Chem setup

S. Archer-Nicholls et al.

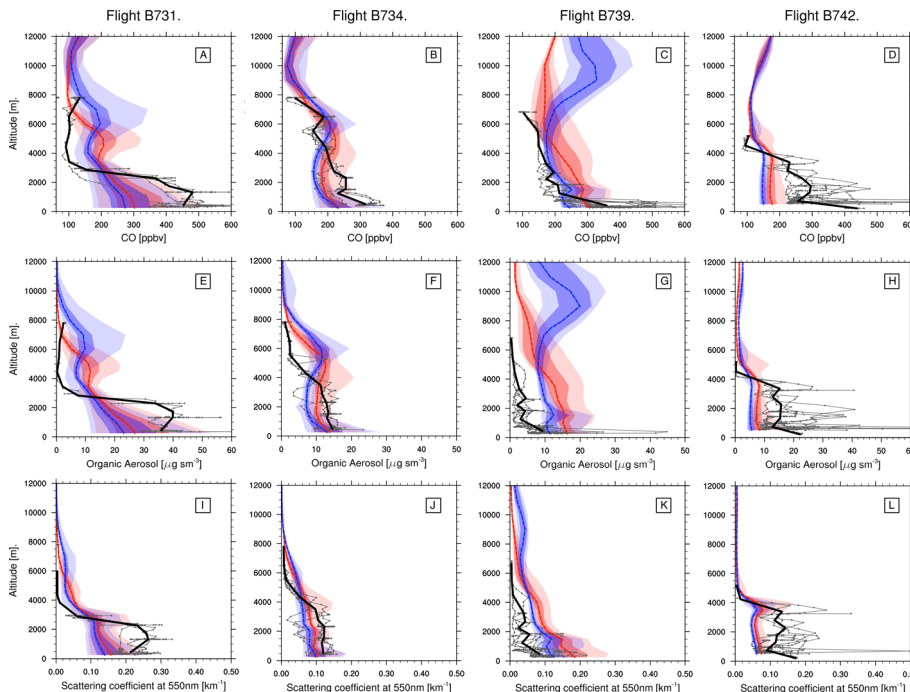


**Figure 8.** Vertical profiles of CO (ppbv), POM ( $\mu\text{g sm}^{-3}$ ) and  $b_{\text{scat}}$  at 550 nm ( $\text{km}^{-1}$ ). (a, e and i) from flight B731 (14 September 2012), (b, f and j) from flight B734 (18 September), (c, g and k) from flight B739 (23 September) and (d, h and l) from flight B742 (27 September). Red dashed lines show median from the modified emissions scenario, with strong red shaded region the interquartile range and the faded region the 5th–95th percentile range. Blue lines and shaded regions are for the standard 3BEM emissions scenario. Solid black line shows median line of profiles conducted by flights, fine grey lines flight measurements averaged over every 3 min.

## SAMBBA WRF-Chem setup

S. Archer-Nicholls et al.

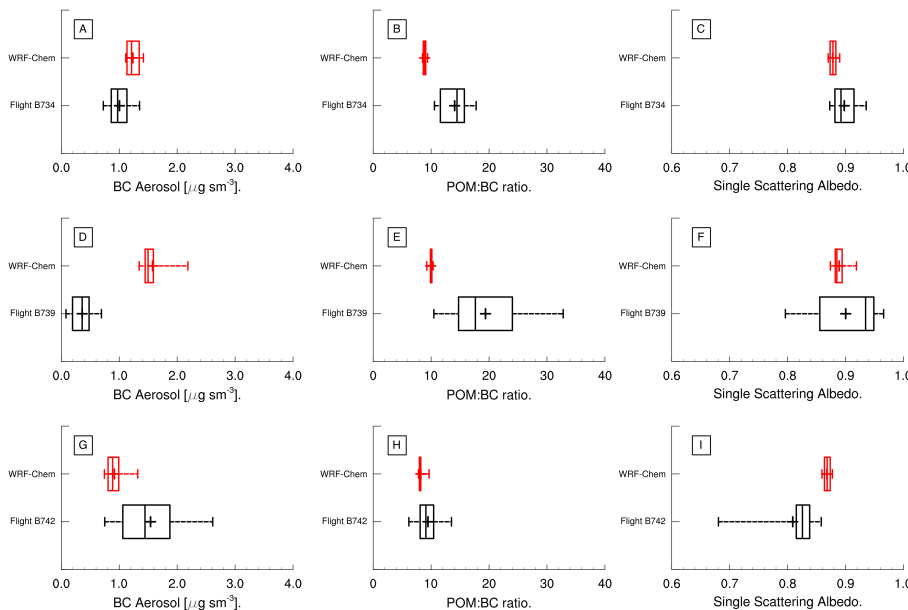


**Figure 9.** Box-whisker plots of black carbon (BC,  $\mu\text{g sm}^{-3}$ ), particulate organic matter to black carbon ratio (POM:BC) and single scattering albedo ( $\omega_0$ ), with bounds of box showing interquartile range, end of dashed lines the 5th and 95th percentiles, and cross over the mean. Showing spread of data from flights and extracted along flight path from modified emissions WRF-Chem run. Screened to only show data from straight-level runs below 3.25 km a.s.l. Flight data averaged over every three minutes (approximately the time taken to travel across one 25 km grid cell). Panels (a, d and g) flight B734 (18 September), panels (b, e and h) flight B739 (23 September) and panels (c, f and i) flight B742 (27 September).

- [Title Page](#)
- [Abstract](#) [Introduction](#)
- [Conclusions](#) [References](#)
- [Tables](#) [Figures](#)
- [◀](#) [▶](#)
- [◀](#) [▶](#)
- [Back](#) [Close](#)
- [Full Screen / Esc](#)
- [Printer-friendly Version](#)
- [Interactive Discussion](#)



# SAMBBA WRF-Chem setup

S. Archer-Nicholls et al.

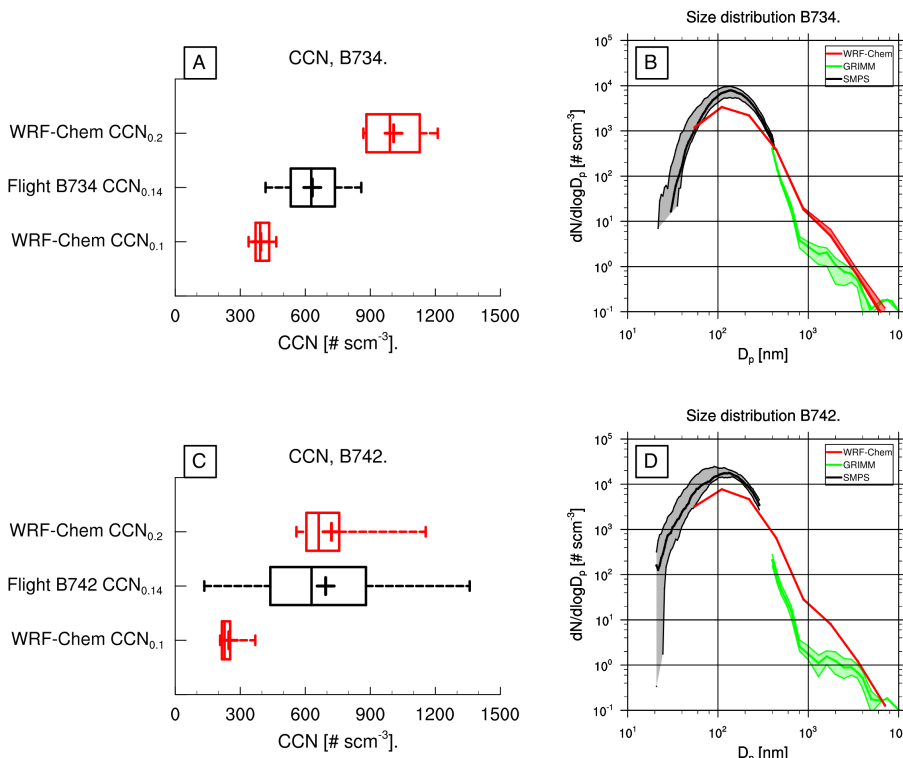


**Figure 10.** Plots of CCN concentration ( $\text{scm}^{-3}$ ) and size distribution  $dN/d\log_{10}(D_p)$  ( $\text{scm}^{-3}$ ). Comparing flight data from flights B734 (**a** and **b**) and B742 (**c** and **d**) with model data from modified emissions run. Model data extracted along flight path and interpolated in vertical axis and in time. CCN plots show CCN concentration at 0.14% supersaturation ( $\text{CCN}_{0.14}$ ) from measurements, with CCN concentrations at 0.1% and 0.2% supersaturation ( $\text{CCN}_{0.1}$ ,  $\text{CCN}_{0.2}$ ) from model. Size distribution shows red line for median WRF-Chem data over 8 MOSAIC size bins. Black line median from SMPS instrument, green line median from GRIMM instrument. Shaded regions show interquartile range.